arXiv:1607.02788v1 [stat.CO] 10 Jul 2016

Parallel local approximation MCMC for expensive models

Patrick R. Conrad*, Andrew D. Davis*, Youssef M. Marzouk*, Natesh S. Pillai†, and Aaron Smith‡

Abstract. Performing Bayesian inference via Markov chain Monte Carlo (MCMC) can be exceedingly expensive when posterior evaluations invoke the evaluation of a computationally expensive model, such as a system of partial differential equations. In recent work [10] we described a framework for constructing and refining *local approximations* of such models during an MCMC simulation. These posterior–adapted approximations harness regularity of the model to reduce the computational cost of inference while preserving asymptotic exactness of the Markov chain. Here we describe two extensions of that work. First, focusing on the Metropolis–adjusted Langevin algorithm, we describe how a proposal distribution can successfully employ gradients and other relevant information extracted from the approximation. Second, we prove that samplers running in parallel can collaboratively construct a shared posterior approximation while ensuring ergodicity of each associated chain, providing a novel opportunity for exploiting parallel computation in MCMC. We investigate the practical performance of our strategies using two challenging inference problems, the first in subsurface hydrology and the second in glaciology. Using local approximations constructed via parallel chains, we successfully reduce the run time needed to characterize the posterior distributions in these problems from days to hours and from months to days, respectively, dramatically improving the tractability of Bayesian inference.

Key words. Markov chain Monte Carlo, parallel computing, Metropolis-adjusted Langevin algorithm, Bayesian inference, approximation theory, local regression, surrogate modeling

AMS subject classifications. 65C40, 62F15, 60J22

1. Introduction.

Markov chain Monte Carlo (MCMC) is a powerful tool for performing Bayesian inference, but can be computationally prohibitive in many settings, especially when posterior density evaluations involve a computationally expensive step. For instance, applications in the physical sciences often require partial differential equation *forward models*, evaluated using numerical solvers with nontrivial run times. When these solvers must be invoked with each posterior evaluation, direct sampling with MCMC can become intractable.

A standard approach to reducing this computational burden for well-behaved problems is to construct an approximation or "surrogate" of the forward model or likelihood function, and then to sample from (or otherwise characterize) the posterior distribution induced by this approximation [42, 25, 39, 43, 34, 33, 3, 24, 27, 7, 15]. Although such approaches can be quite effective at reducing computational cost, they may be difficult to use in practice—in part because they separate the construction of the surrogate from the subsequent inference procedure. Approximation of the forward model biases posterior expectations [11] in a way that cannot easily be quantified. It is then difficult to decide how much computational effort should be devoted to surrogate construction, and how to balance the resulting biases with the statistical errors of posterior sampling. Alternatives such as delayed-acceptance MCMC

*Massachusetts Institute of Technology, Cambridge, MA 02139, USA, {prconrad, davisad, ymarz}@mit.edu.

†Harvard University, Cambridge, MA 02138, USA, pillai@stat.harvard.edu.

‡University of Ottawa, Ottawa, ON K1N 7N5, Canada, asmi28@uottawa.ca.

[8, 14] yield asymptotically exact sampling, but surrender potential speedups by requiring at least one evaluation of the forward model for each accepted sample. In recent work [10], we demonstrated that surrogate construction and posterior exploration can instead be *joined*, yielding a framework for incrementally and infinitely refining a surrogate during MCMC sampling. This framework allows the approximation to be tailored to the problem—e.g., made most accurate in regions of high posterior probability—while guaranteeing that the associated Markov chain asymptotically samples from the *exact* posterior distribution of interest. Empirical studies on problems of moderate dimension showed that the number of expensive posterior evaluations per MCMC step can be reduced by orders of magnitude, with no discernable loss of accuracy in posterior expectations.

This work describes two key extensions of the framework in [10]. First, we show that our approximation scheme enables a novel type of MCMC parallelism: concurrent chains can collaboratively develop a *shared* approximation. Effectively exploiting parallel computation in MCMC is often challenging because the core algorithm is inherently sequential, but our strategy directly deploys parallel resources to address the key performance bottleneck: the cost of repeatedly running the forward model.

Second, while our previous work showed how to build a convergent approximation of the target probability density, it did not support the idea of using this approximation to construct a proposal distribution. MCMC performance is highly dependent on the choice of proposal, but sophisticated proposals, such as the Metropolis-adjusted Langevin algorithm (MALA) and its manifold variants [20], can be expensive to apply because they require gradients (and possibly higher derivatives) of the forward model. This derivative information is often expensive or impossible to compute directly, but is trivial to extract from an approximation. Intuitively, it should then be possible to use our approximation framework to greatly reduce the costs of such proposals. Here we do exactly that, extending our previous theoretical results to show that the Monte Carlo estimates obtained by our algorithm converge to the correct value, as long as the convergence of our approximation to the target distribution yields convergence of the associated approximate Markov transition kernel in a suitably strong norm. As an example, we show how to use simplified manifold MALA within our local approximation scheme, and prove that the resulting stochastic process is convergent in a representative case.

Finally, we construct two synthetic inference problems that are representative of interesting scientific queries, that involve computationally expensive forward models (such that naïve use of the model in sampling would take days or months), and that have nontrivial posterior structure which must be characterized using MCMC. The first is a problem in groundwater hydrology, where a subsurface conductivity field is inferred from observations of tracer transport; it is a more complex and realistic version of the linear elliptic PDE inverse problem [16], combining an elliptic equation for the hydraulic head with another PDE governing tracer dispersion [17, 35]. The second problem is drawn from glaciology: here we infer the basal friction parameters of a shallow-shelf ice stream model [29, 30, 31] from observations of surface ice velocity. Our numerical experiments evaluate MCMC efficiency, accuracy, and wallclock time, and benchmark the parallel performance of our algorithms. Results demonstrate strong performance of our approach; for example, inference in the ice stream model becomes tractable, with the time needed to characterize the posterior reduced from roughly two months to just over a day.

The remainder of this paper is organized as follows. Section 2 reviews the basic algorithmic framework of local approximation MCMC. Section 3 presents and analyzes the shared construction of approximations for parallel MCMC. Section 4 describes the use of local approximations in the proposal scheme, and Section 5 describes our numerical experiments. Proofs of the main convergence results, along with certain algorithmic details, are deferred to the appendices.

2. Review of local approximation MCMC. We are interested in Bayesian inference problems with posterior densities of the form

$$p(\theta|\mathbf{d}) \propto \ell(\theta|\mathbf{d},\mathbf{f})p(\theta),$$

for parameters $\theta \in \Theta \subseteq \mathbb{R}^d$, data $\mathbf{d} \in \mathbb{R}^n$, a forward model $\mathbf{f} : \Theta \to \mathbb{R}^n$, and probability densities specifying the prior $p(\theta)$ and likelihood function ℓ. The forward model may enter the likelihood function in various ways. For instance, if $\mathbf{d} = \mathbf{f}(\theta) + \eta$, where η represents some measurement or model error with probability density p_η, then $\ell(\theta|\mathbf{d},\mathbf{f}) = p_\eta(\mathbf{d}-\mathbf{f}(\theta))$.

Assume that the forward model is both *computationally expensive* and a *black box*, so that we cannot inspect or modify it. In this setting, standard approaches to MCMC are likely to be limited by the computational expense of evaluating the forward model at every step of the chain. Our approach addresses this cost by storing the results of each model evaluation in a set $\mathcal{S}_t := \{(\theta_i, \mathbf{f}(\theta_i))\}_{i=1}^{n_t}$ and reusing them. The stochastic process $\{\theta_t\}_{t\geq 0}$ proposed in [10] evolves by drawing new points from some proposal kernel q and accepting or rejecting the proposed move according to an approximation of the forward model, $\tilde{\mathbf{f}}_t$, constructed from the set $\mathcal{S}_t$. During the simulation of this process, the algorithm carefully chooses new points at which to run the forward model, enlarging $\mathcal{S}_t$ and thus improving $\tilde{\mathbf{f}}_t$. Intuitively, it would seem that if $\tilde{\mathbf{f}}_t$ converges to $\mathbf{f}$ in an appropriate sense, then the sequence $\{\theta_t\}_{t\geq 0}$ might asymptotically behave like the usual Metropolis-Hastings chain with proposal q and forward model $\mathbf{f}$. Indeed, the algorithm we constructed in [10] has these properties.

We obtain a converging sequence of approximations $\tilde{\mathbf{f}}_t$ by constructing the approximation locally—that is, constructing $\tilde{\mathbf{f}}_t(\theta)$ using only a small subset of $\mathcal{S}_t$ for which the stored input lies within a distance R of θ. Local approximations are relatively straightforward to analyze, in that they typically converge whenever the sample set becomes denser, allowing $R \to 0$. (Regularity conditions on $\mathbf{f}$ sufficient for convergence in the case of local polynomial approximations, for example, are given in [9].) These general conditions for convergence allow us to promote efficiency by aggressively tailoring $\mathcal{S}_t$ during sampling, while still maintaining asymptotic exactness of the overall MCMC. The resulting algorithm is straightforward to use, since its adaptivity allows users to treat it much like standard adaptive MCMC algorithms: the behavior of the chain can be monitored for convergence, which in our case reflects both the exploration of the posterior and the convergence of the approximation. Our work thus differs from previous efforts using global approximations to accelerate inference [34, 3, 24, 43], where the entire set $\mathcal{S}_t = \mathcal{S}_0$ is constructed as a preprocessing step and is used to build a single high-order approximation. In these methods it is difficult to choose how many samples $\mathcal{S}_0$ should contain or how to monitor the accuracy of the overall sampling.

An illustration of the algorithm is given in Figure 2.1. At early times, the samples are sparse, leading to local models constructed over large regions, depicted by large balls, ren-

dering them relatively inaccurate. As MCMC progresses, refinements increase the density of the sample set in regions of high posterior probability, shrinking the local neighborhoods and increasing the quality of approximations. Model runs do not lie on any structured grid and are generally contained within regions of the parameter space that are relevant to the inference problem, thus enhancing efficiency whenever the posterior is concentrated.

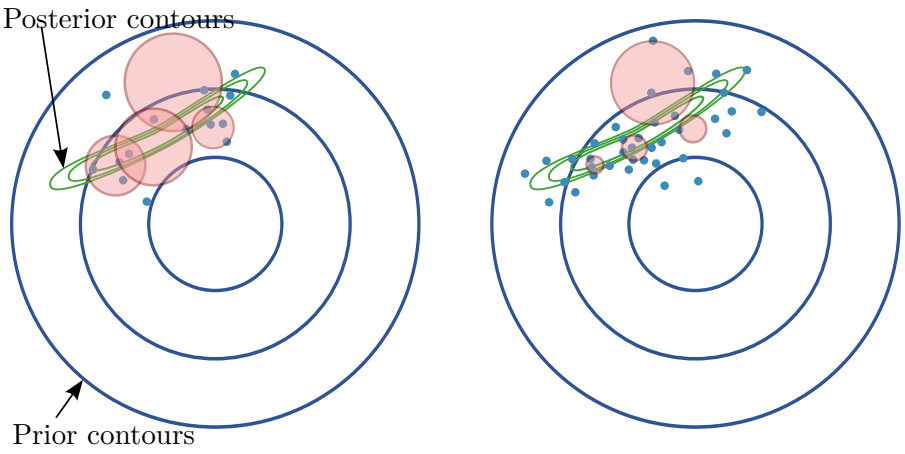

(a) Early times. (b) Late times.

Figure 2.1. *Schematic of the behavior of local approximation MCMC. The balls are centered at locations where local models might be needed, and their radii indicate the size of the sample set; the accuracy of local models generally increases as this ball size shrinks. At early times the sample set is sparse and thus local approximations are built over relatively large balls, implying that their accuracy is limited. At later times refinements enrich the sample set in regions of high posterior probability, allowing the local models to shrink and become more accurate.*

We now review a sketch of our approximate MCMC algorithm, given in Algorithm 2.1 and previously described in [10]. For a complete description of our algorithm, we refer readers to our previous work and to Appendix A. The stochastic process $\{\theta_t\}_{t\geq 0}$ is produced by the method RunChain, which applies the transition kernel K_t repeatedly. The transition kernel is provided with the current state of the chain θ_t; the current set of samples $\mathcal{S}_t$; the inference problem, as defined by ℓ, $\mathbf{d}$, p, and $\mathbf{f}$; and a symmetric translation–invariant proposal distribution q.

The kernel uses the current point of the chain, θ^-, to draw a proposal, θ^+. It forms local approximations near these points, $\tilde{\mathbf{f}}^+$ and $\tilde{\mathbf{f}}^-$, respectively, based on nearby samples contained in $\mathcal{S}_t$. Next, it computes the acceptance probability α in the usual way, substituting the approximations for the true forward model. Then, the algorithm optionally refines the sample set by choosing a new point θ^* and running the forward model at that location.

Choosing when and where to refine $\mathcal{S}_t$ is critical to the performance of the overall algorithm. We combine two criteria to decide when to refine the approximation. First, the approximation is refined near θ^- or θ^+ with equal probabilities β_t, such that the expected number of refinements diverges as $t \to \infty$. This criterion is sufficient for convergence of the algorithm, as detailed in [10]. The sequence (β_t) may be difficult to tune in practice, however. Thus we complement the random refinement criterion with a cross–validation strategy that triggers refinement whenever the estimated error in the acceptance probability

Algorithm 2.1 Sketch of approximate Metropolis-Hastings algorithm

1: **procedure** RunChain($\theta_1, \mathcal{S}_1, \ell, \mathbf{d}, p, \mathbf{f}, q, T$)
2: **for** $t = 1 \dots T$ **do**
3: $(\theta_{t+1}, \mathcal{S}_{t+1}) \leftarrow K_t(\theta_t, \mathcal{S}_t, \ell, \mathbf{d}, p, \mathbf{f}, q)$
4: **end for**
5: **end procedure**

6: **procedure** $K_t(\theta^-, \mathcal{S}, \ell, \mathbf{d}, p, \mathbf{f}, q)$
7: Draw proposal $\theta^+ \sim q(\theta^-, \cdot)$
8: Compute approximate models $\tilde{\mathbf{f}}^+$ and $\tilde{\mathbf{f}}^-$, valid near θ^+ and θ^-, respectively.
9: Compute acceptance probability $\alpha \leftarrow \min\left(1, \frac{\ell(\theta|\mathbf{d},\tilde{\mathbf{f}}^+)p(\theta^+)}{\ell(\theta|\mathbf{d},\tilde{\mathbf{f}}^-)p(\theta^-)}\right)$
10: **if** approximation needs refinement near θ^- or θ^+ **then**
11: Select new point θ^* and grow $\mathcal{S} \leftarrow \mathcal{S} \cup (\theta^*, \mathbf{f}(\theta^*))$. Repeat from Line 8.
12: **else**
13: Draw $u \sim \text{Uniform}(0, 1)$. If $u < \alpha$, **return** $(\theta^+, \mathcal{S})$; else **return** $(\theta^-, \mathcal{S})$.
14: **end if**
15: **end procedure**

α appears too large. This latter threshold for refinement is tightened with increasing t, pushing the approximation to improve as the chain lengthens. Although the cross–validation criterion is not sufficient for convergence of the algorithm, it appears efficient in practice, and we use it in conjunction with the random refinement strategy. When refinement is needed near either of θ^- or θ^+, we do not simply run the model at that point, since doing so would introduce clusters into $\mathcal{S}_t$, degrading the quality of local approximations. Instead, we use a local space-filling design strategy to choose a distinct but nearby point θ^* at which to run the model.

3. Sharing local approximations for parallel MCMC. The naïve approach to parallelizing MCMC is simply to run several independent chains in parallel. Although running parallel chains facilitates useful convergence diagnostics [12, 4], practical scaling in highly parallel environments is limited because of the serial nature of MCMC and the replication of transient behavior across multiple chains [41].

More sophisticated strategies for parallel MCMC exchange information between the chains, for example by proposing moves to states discovered by other chains [13]. Population MCMC algorithms explore a family of tempered distributions with parallel chains, so that swapping states between the chains can provide long-range moves [6]. These techniques attempt to improve the mixing time of the Markov chain, and when successful, may provide superior performance to the naïve parallelization. Other constructions [5] propose multiple points in parallel, and try to make use of all these points in determining subsequent steps of a single chain.

Any of these parallel approaches requires repeated evaluations of the forward model, however, which can dominate the overall cost of the algorithm. If multiple copies of Algorithm 2.1 are run in parallel, a natural idea is to allow them to collaborate by sharing a common set of evaluations $\mathcal{S}_t$. That is, whenever one chains performs refinement, the

result is shared asynchronously with all the chains; hence each chain receives additional model evaluations "for free." Since the limiting computational cost in our context lies in constructing $\mathcal{S}_t$, parallelizing this process should directly impact the real-world performance of the sampler during both the burn-in and the stationary phases of the chains. Although it should be straightforward to combine parallelization of $\mathcal{S}_t$ with other information exchanges between parallel chains, we leave that as future work.

3.1. Convergence of the parallel algorithm. Fortunately, the sufficient conditions for convergence of the "single-chain" version of Algorithm A.3 described in [10] are also sufficient conditions for the convergence of the parallel version. The arguments given in [10] are straightforward to extend because we have already chosen conditions where enlarging the sample set $\mathcal{S}_t$ is always helpful; thus the additional refinements contributed by parallel chains cannot hinder convergence. Rather than repeating the entire discussion of convergence from that paper, here we merely extend the simplest and weakest convergence result—for a single chain on a compact state space—to the case of parallel chains. We refer the reader to [10] for related conditions and a treatment of non-compact state spaces that can similarly be extended to the parallel case.

We require some notation before stating the result. Denote by $\mathcal{L}(X)$ the distribution of a random variable X. For fixed $\epsilon > 0$, we say that $\mathcal{S} \subset \Theta$ is an ϵ-cover of Θ if $\sup_{\theta\in\Theta} \min_{s\in\mathcal{S}} \|\theta - s\|_2 < \epsilon$. We note that if Steps 13–21 and Step 23 are removed from Algorithm A.3, and all references to $\mathcal{S}_t$ are replaced by a reference to a single set $\mathcal{S}$, then the sequence $\{\theta_t\}_{t\geq 0}$ constructed by running the modified algorithm is a Markov chain. We use the $\mathcal{S}$ subscript to denote all approximate objects associated with this Markov chain (e.g., $K_\mathcal{S}$ is the associated transition kernel, $r_\mathcal{S}$ is the proposal function from Step 9 of Algorithm A.3 and $q_\mathcal{S}$ is the associated proposal density, $p_\mathcal{S} := \ell(\theta|\mathbf{d}, \tilde{\mathbf{f}})p(\theta)$ is the approximation to $\ell(\theta|\mathbf{d}, \mathbf{f})p(\theta)$ used in Step 11 of Algorithm A.3, and $\alpha_\mathcal{S}$ is the associated acceptance probability). Similarly, K_∞, r_∞, q_∞, p_∞, and α_∞ are the values of these objects for the Markov chain with the same proposal kernel as in Algorithm A.3 and with the *correct* posterior distribution as its target distribution. Finally, define $\pi(\theta) := p(\theta)\ell(\theta|\mathbf{d}, \mathbf{f})/Z$, where Z is a normalization constant. Our simple result makes the following assumptions:

Definition 3.1 (Sufficient conditions for convergence).

1. *The state space Θ is compact.*
2. *The proposal $q(\theta, \cdot\,|\,\mathbf{f}) = q(\theta, \cdot)$ does not depend on $\mathbf{f}$, and both the proposal distribution $q(\theta, \cdot)$ and target distribution $p(\cdot|\,\mathbf{d})$ have C^∞ densities that are bounded away from zero uniformly in θ.*
3. *The sequence of parameters $\{\beta_t\}_{t\in\mathbb{N}}$ used in Algorithm A.3 are of the form $\beta_t \equiv \beta > 0$; any sequence $\{\gamma_t\}_{t\geq 0}$ is allowed.*
4. *The approximation of $\log p(\theta|\mathbf{d})$ is made via quadratic interpolation on the $N = (d+1)(d+2)/2$ nearest points.*
5. *The sub-algorithm* RefineNear *is replaced with:*
$$\textsc{RefineNear}(\theta, \mathcal{S}) = \textbf{\textit{return}}(\mathcal{S} \cup \{(\theta, f(\theta))\}).$$
6. *We fix a constant $0 < \lambda < \infty$. In Step 15, immediately before the word **then**, we add '**or**, for $\mathcal{B}(\theta^+, R)$ as defined in the subalgorithm* LocApprox$(\theta^+, \mathcal{S}, \emptyset)$ *used in Step 8, the collection of points $\mathcal{B}(\theta^+, R) \cap \mathcal{S}$ is not λ-poised.' We add the same check, with θ^- replacing θ^+ and 'Step 10' replacing 'Step 8,' in Step 17. The concept of poisedness is defined in [9].*

The following result extends Theorem 3.4 of [10] to parallel chains.

Theorem 3.2 (Convergence with parallel chains). *Let $\{X_t^{(i)}\}_{t\geq 0,\, 1\leq i\leq n}$ be the n stochastic processes obtained in a parallel run of Algorithm A.3 with n chains, and assume that the algorithm parameters satisfy Assumption 3.1. Then, for all $1 \leq i \leq n$,*

$$\lim_{t\to\infty} \|\mathcal{L}(X_t^{(i)}) - \pi\|_{TV} = 0.$$

Proof. The proof of Lemma B.3 of [10] holds exactly as stated, with the proof as given. The remainder of the proof of Theorem 3.4 from [10] holds for $\{X_t^{(i)}\}_{t\geq 0}$, for each fixed $1 \leq i \leq n$, with the following modifications:

(i) The chain $\{X_t\}_{t\geq 0}$ should be replaced by $\{X_t^{(i)}\}_{t\geq 0}$ wherever it appears; and

(ii) The auxillary process associated with $\{X_t^{(i)}\}_{t\geq 0}$ is $\left\{\left(\mathcal{S}_t, X_t^{(1)}, \ldots, X_t^{(i-1)}, X_t^{(i+1)}, \ldots, X_t^{(n)}\right)\right\}_{t\geq 0}$, rather than $\{\mathcal{S}_t\}_{t\geq 0}$. ■

We emphasize that this proof of the convergence of $\{X_t^{(i)}\}_{t\geq 0}$ is completely indifferent to the points that are added to $\mathcal{S}_t$ by the other chains $\{X_t^{(j)}\}_{t\geq 0}$, $j \neq i$.

Remark 3.3 (Do parallel chains always work?). *Although our sufficient conditions for convergence carry over to the parallel case, it is natural to ask whether there are any problems that are not covered by our current theory—i.e., where, having departed from the sufficient conditions of Definition 3.1, the single-chain algorithm still converges but the parallel algorithm does not. We conjecture that the answer is no, but are unable to prove it.*

To explain the difficulty in proving this conjecture, note that all the proofs of sufficient conditions for convergence given in [10] apply as stated to the parallel version of Algorithm A.3 because they proceed by proving the following critical steps:

1. *Due to minorization conditions (e.g., the second condition of Assumption 3.1), for any $\epsilon > 0$ the set $\mathcal{S}_t$ will be an ϵ-cover of Θ for all t sufficiently large.*
2. *The distance $\|K_\infty(\theta_t, \cdot) - K_{\mathcal{S}_t}(\theta_t, \cdot)\|_{TV}$ between a single 'step' of Algorithm A.3 and the step that would be made by the true transition kernel K_∞ can be made arbitrarily small by making $\mathcal{S}_t$ an ϵ-cover of Θ for ϵ sufficiently small.*

In particular, under the assumptions made in [10], adding points to $\mathcal{S}_t$ cannot hurt the convergence of $\{X_t^{(i)}\}_{t\geq 0}$ very much, because adding points to an ϵ-cover always results in a set that is still an ϵ-cover. For a sufficiently broad class of Metropolis-Hastings chains, however, it is not *true that $K_{\mathcal{S}}$ is close to K_∞ whenever $\mathcal{S}$ is an ϵ-cover, and in particular it is possible to* add *points to $\mathcal{S}$ while simultaneously making an approximation worse. This possibility of mal-adaption is what makes adaptive algorithms difficult to study, and prevents us from making the stronger claim that the parallel algorithm is convergent under every possible condition where the single-chain algorithm is.*

Remark 3.4 (Do parallel chains have better properties?). *As with algorithms that exchange states between parallel chains, we believe that, in general, the parallel version of our algorithm will have better convergence properties than the original algorithm. Running many chains in parallel allows better initial exploration and allows for better recovery from poor initial choices. It is possible to construct simple examples formalizing this benefit, but broad characterization of the additional robustness stemming from parallelization in MCMC is an open problem.*

4. Local approximations and approximating the proposal. We now show how the transition kernel of our approximate MCMC scheme can use the current approximation not only to evaluate the acceptance probability, but also to construct a proposal distribution. This development enables a much wider range of Metropolis-Hastings proposals to be used with expensive models, and in particular allows gradient- and Hessian-driven proposals to be used in a setting where derivatives of $\mathbf{f}$ cannot be directly evaluated. We proceed by recalling the Metropolis-adjusted Langevin algorithm (MALA) algorithm and explaining how to adapt local approximations to this proposal scheme. Next, we prove a general result that our modified algorithm is still convergent as long as the good properties of the approximation are transferred into good approximation of the overall kernel. We conclude by showing that the result applies in the representative case of manifold MALA.

4.1. Simplified manifold Metropolis-adjusted Langevin algorithm (MALA). The simplified manifold Metropolis-adjusted Langevin algorithm (mMALA) [20] is a recent method for constructing proposals adapted to the local geometry of the target distribution. This method is also closely related to the preconditioning performed in the stochastic Newton method [32]. The mMALA proposal is derived by explicitly discretizing a Langevin diffusion with stationary distribution $p(\theta|\mathbf{d})$, leading to

$$q(\theta, \theta'|\mathbf{f}) = \mathcal{N}\left(\theta'; \theta + \frac{\epsilon}{2} M(\theta) \nabla_\theta \log\left(\ell(\theta|\mathbf{d}, \mathbf{f}) p(\theta)\right), \epsilon M(\theta)\right), \tag{4.1}$$

for integration step size ϵ and position-dependent symmetric positive definite (SPD) mass matrix $M(\theta)$, which we may treat as a preconditioner. We use the notation $q(\theta, \theta'|\mathbf{f})$ to emphasize the dependence of the proposal on the forward model. The corresponding acceptance ratio is

$$\alpha(\theta, \theta') = \min\left(1, \frac{\ell(\theta'|\mathbf{d}, \mathbf{f}) p(\theta') q(\theta', \theta|\mathbf{f})}{\ell(\theta|\mathbf{d}, \mathbf{f}) p(\theta) q(\theta, \theta'|\mathbf{f})}\right).$$

We are relatively unconstrained in our choice of preconditioner, as long as it is SPD. Standard MALA corresponds to choosing the identity matrix, $M(\theta) = I$. Simplified manifold mMALA [20], on the other hand, chooses the mass matrix to reflect a Riemannian metric induced by the posterior distribution:

$$M(\theta) = \left[-\mathbb{E}_{\mathbf{d}|\theta}\left(\nabla_\theta^2 \log \ell(\theta|\mathbf{d}, \mathbf{f})\right) - \nabla_\theta^2 \log p(\theta)\right]^{-1}.$$

The inverse of this matrix is the expected Fisher information plus the negative Hessian of the log-prior density. In general, computing the expected Fisher information is not trivial, but it is relatively simple for Gaussian likelihoods, e.g.,

$$\ell(\theta|\mathbf{d}, \mathbf{f}) = \mathcal{N}(\mathbf{d}; \mathbf{f}(\theta), \Sigma_\ell),$$

for some covariance matrix $\Sigma_\ell \in \mathbb{R}^{n \times n}$. If we also have a Gaussian prior, $p(\theta) = \mathcal{N}(\theta; \mu, \Sigma_p)$, with covariance $\Sigma_p \in \mathbb{R}^{d \times d}$ and mean vector $\mu \in \mathbb{R}^d$, then

$$M^{-1}(\theta) = J(\theta)^\top \Sigma_\ell^{-1} J(\theta) + \Sigma_p^{-1},$$

where $J(\theta) := \nabla_\theta \mathbf{f}(\theta) \in \mathbb{R}^{n\times d}$. Girolami *et al.* [20] observe that choosing the preconditioner in this manner can dramatically improve the performance of MALA. Yet even standard MALA can be difficult to apply in practice because the necessary derivatives must be computable and inexpensive; the manifold variant uses Jacobians of the forward model, which are typically even more challenging to obtain. Adapting mMALA and similar proposals to use local approximation is therefore particularly interesting, as approximations can cheaply provide these derivatives.

4.2. Modifying the algorithm. The key challenge in extending Algorithm 2.1 to mMALA (and similar proposals) is to allow simultaneous use of the approximation within the proposal and the acceptance probability. Algorithm 4.2 shows the three required changes. Two modifications are trivial: we restore the proposal distribution to its usual place in the acceptance probability, to account for the non-symmetric proposal; and we provide the proposal with the approximate forward model $\tilde{\mathbf{f}}$.

The third step is more subtle, introducing a coupling construction to allow model refinement to proceed safely. Note that in Algorithm 2.1, refinement only recomputes the acceptance probability; the proposed point is held fixed. Hence, exactly one proposal is made per step, even though an inaccurate approximation might cause the algorithm to seek further information before deciding whether that proposal can be accepted. Allowing a new proposal to be generated upon refinement would bias the chain away from regions with inaccurate approximations (equivalently, towards regions where the approximation appears accurate), which is clearly undesirable.

This difficulty can be resolved by coupling the approximate kernel K_t to the kernel associated with the true model, K_∞. We accomplish this coupling by fixing the realization of the random variable used to generate the proposal, but allowing the proposal to be recomputed if the model is refined. (See [38, 18] for other algorithms that re-use randomness to avoid bias, and [45] for a typical use of this idea in a theoretical paper.) Specifically, construct a deterministic function $r(\theta, \mathbf{z}, \mathbf{f})$ such that drawing a random vector $\mathbf{z} \sim \mathcal{N}(0, I)$[1] and then computing $\theta' = r(\theta, \mathbf{z}, \mathbf{f})$ is equivalent to drawing $\theta' \sim q(\theta, \cdot|\mathbf{f})$. The modified algorithm holds $\mathbf{z}$ fixed under refinement, recomputing θ^+ as needed. In the case of standard Metropolis-Hastings proposals, this coupling strategy reduces to our original approach. This coupling construction ensures that the magnitude of any perturbation to the proposed point θ^+ induced by refinement vanishes as $t \to \infty$.

In the case of simplified manifold MALA, the proposal will be a Gaussian distribution, $q(\theta, \theta'|\mathbf{f}) = \mathcal{N}\left(\mu_q(\theta, \mathbf{f}), \Sigma_q(\theta, \mathbf{f})\right)$, for some position- and model-dependent mean and covariance, and hence $r = \mu_q(\theta, \mathbf{f}) + \Sigma_q^{1/2}(\theta, \mathbf{f})\mathbf{z}$. The rest of the algorithm is updated naturally, including the inclusion of the proposal into the cross-validation criterion. The resulting approach is summarized in Algorithm 4.2. For brevity, we defer precise pseudocode to Algorithm A.3 in Appendix A.

4.3. Convergence analysis. We now provide a convergence result for our generalized Algorithm A.3. Some technical definitions and the proofs from this section may be found in Appendix B.

[1] We choose a vector of independent standard Gaussians for convenience and without loss of generality, but in practice other distributions for $\mathbf{z}$ may be more convenient.

Algorithm 4.2 Sketch of approximate Metropolis-Hastings algorithm with general proposals

procedure $K_t(\theta^-, \mathcal{S}, \ell, \mathbf{d}, p, \mathbf{f}, r, q)$
  Draw $\mathbf{z}_t \sim \mathcal{N}(0, I)$
  Construct $\tilde{\mathbf{f}}^-$
  Compute $\theta^+ = r(\theta^-, \mathbf{z}_t, \tilde{\mathbf{f}}^-)$
  Construct $\tilde{\mathbf{f}}^+$
  Compute acceptance probability $\alpha \leftarrow \min\left(1, \frac{\ell(\theta^+|\mathbf{d},\tilde{\mathbf{f}}^+)p(\theta^+)q(\theta^+,\theta^-|\tilde{\mathbf{f}}^+)}{\ell(\theta^-|\mathbf{d},\tilde{\mathbf{f}}^-)p(\theta^-)q(\theta^-,\theta^+|\tilde{\mathbf{f}}^-)}\right)$
  if approximation needs refinement near θ^- or θ^+ **then**
    Select new point θ^* and grow $\mathcal{S} \leftarrow \mathcal{S} \cup (\theta^*, \mathbf{f}(\theta^*))$. Repeat from Line 3.
  else
    Draw $u \sim \text{Uniform}(0, 1)$. If $u < \alpha$, **return** $(\theta^+, \mathcal{S})$, else **return** $(\theta^-, \mathcal{S})$.
  end if
end procedure

The general idea is to show that as the sample set $\mathcal{S}_t$ becomes dense, the approximate kernel $K_{\mathcal{S}}$ converges to the kernel using the true model, K_∞, and that MCMC converges as a result. We begin by stating our assumptions precisely. Below W_2 denotes the 2-Wasserstein metric, defined in Appendix B.

Definition 4.5 (Convergence assumptions). *Assume that:*

1. *For any $\delta > 0$, there is an $\epsilon = \epsilon(\delta) > 0$ so that any ϵ-cover $\mathcal{S}$ satisfies*

$$\sup_{\theta \in \Theta} W_2(K_{\mathcal{S}}(\theta, \cdot), K_\infty(\theta, \cdot)) < \delta. \tag{4.2}$$

2. *There exist constants $0 < \eta_0 < \infty$ and $1 < C < \infty$ such that for any $0 < \eta < \eta_0$,*

$$\sup_{\theta, \theta' \in \Theta,\, \|\theta - \theta'\| < \eta} W_2(K_\infty(\theta, \cdot), K_\infty(\theta', \cdot)) < C\eta. \tag{4.3}$$

3. *For any $\varphi_0 < \infty$ and $\delta > 0$, there exists $\epsilon > 0$ so that any ϵ-covers $\mathcal{S}$, $\mathcal{S}'$ satisfy*

$$\sup_{\|z\| \le \varphi_0} \sup_{\theta \in \Theta} \|r_{\mathcal{S}}(\theta, z) - r_{\mathcal{S}'}(\theta, z)\| \le \delta. \tag{4.4}$$

4. *Assumptions 3.1 hold.*

The following theorem states that these assumptions, which we will have to check, are sufficient for convergence of the approximate Markov chain.

Theorem 4.6 (Convergence of Algorithm A.3 on compact state space). *Let Assumptions 4.5 hold and let $\{X_t\}_{t \ge 0}$ be the sequence drawn from a run of Algorithm A.3. Then*

$$\lim_{t \to \infty} W_2(\mathcal{L}(X_t), \pi) = 0. \tag{4.5}$$

Remark 4.7. *The proof proceeds by coupling each step of the output of Algorithm A.3. Our coupling construction gives us the important estimate (B.13), which would not hold if the randomness at each step were resampled upon model refinement. In most cases, including our application to mMALA, this proof can be extended to give convergence in total variation distance by using a 'one-shot' coupling (see [40]).*

Finally, we observe that mMALA often satisfies Assumptions 4.5. Although our convergence results only apply to some uses of mMALA, we believe they are representative of the more general case, and suggest the feasibility of analytically transferring the good properties of the approximation onto the kernel.

Theorem 4.8 (Convergence of approximate mMALA). *We consider running Algorithm A.3 with proposal kernel q given by the mMALA algorithm. Assume that:*

(i) *The state space Ω is the d-dimensional torus $[0,1]^d$ for some $d \in \mathbb{N}$.*

(ii) *The mass matrix $M(\theta)$ and likelihood $\ell(\theta|\mathbf{d},\mathbf{f})$ are both C^∞ functions on Ω. Furthermore, the smallest singular value of $M(\theta)$, as well as the first two derivatives of the likelihood $\ell(\theta|\mathbf{d},\mathbf{f})$, are uniformly bounded away from zero by some $c > 0$.*

(iii) *The posterior density $p(\cdot|\mathbf{d})$ is C^∞ and bounded away from zero uniformly on Ω.*

(iv) *Items 3 through 6 of Assumption 3.1 hold.*

Then the output $\{X_t\}_{t\geq 0}$ of Algorithm A.3 satisfies

$$\lim_{t\to\infty} \|\mathcal{L}(X_t) - \pi\|_{TV} = 0.$$

The proof of Theorem 4.8, given in Appendix B, merely checks Assumptions 4.5. Essentially, these assumptions hold because mMALA uses approximations of the derivatives of $\mathbf{f}$ to construct a Gaussian proposal; the derivative approximations improve as $\mathcal{S}$ grows and the Gaussian proposal is not too sensitive to errors in these approximations, and hence the entire kernel converges in the necessary sense.

5. Numerical experiments.

We now apply the parallel local approximation scheme, using both adaptive Metropolis and mMALA proposals, to two computationally intensive inference problems. The first, while expensive, allows us to compare results with reference MCMC chains that employ no approximation, so that we can verify the accuracy of posterior expectations. The second example is more expensive, such that MCMC is intractable without the use of approximations; thus, it demonstrates how parallel local approximations can make fully Bayesian inference feasible in problems where it would otherwise be out of reach.

5.1. Tracer transport problem.

Predicting the evolution of groundwater contaminant concentrations over time is vital to many monitoring and remediation efforts [35]. A contaminant is typically modeled as a non-reactive tracer that diffuses and is advected by groundwater flow. Here we construct an inverse problem that simulates a monitoring configuration: the tracer concentration is observed at a small number of wells over a short period of time, and the subsurface conductivity field must be inferred given these data.

We consider a problem domain with two horizontal coordinates $x, y \in [0,1]^2$. The conductivity field is assumed to be piecewise constant in six irregularly-shaped areas, reflecting different subsurface features (e.g., sand, clay, gravel) each with constant but unknown conductivities. The true log-conductivity is depicted in Figure 5.2. The conductivity is parameterized as

$$\kappa(x,y) = \exp \theta_{\underline{j}(x,y)},$$

where $\underline{j}(x,y) \in \{1,2,\ldots,6\}$ is the smallest integer j such that $x_0^j \leq x \leq x_1^j$ and $y_0^j \leq y \leq y_1^j$, where the bounds $(x_0^j, x_1^j, y_0^j, y_1^j)$ are given Table 5.1. The parameters θ_i are endowed with independent normal priors: $\theta_1 \sim \mathcal{N}(.5,1)$, and $\theta_i \sim \mathcal{N}(1,1)$ for $i = 2,\ldots,6$.

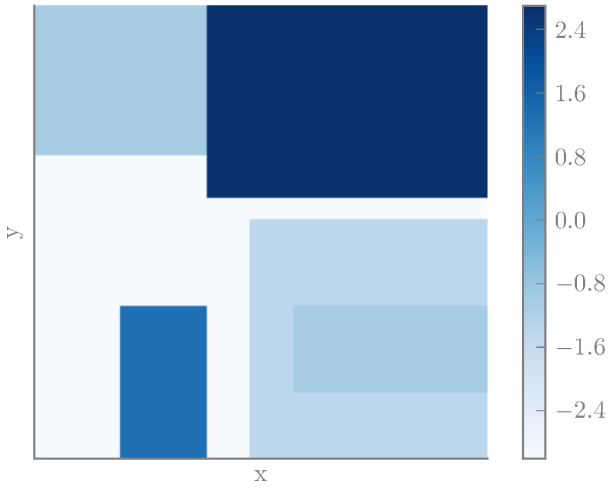

Figure 5.2. *The "true" log-conductivity field.*

Table 5.1

The geometry of the parameters in the tracer problem. The log-conductivity at location (x, y) *is* $\theta_{\underline{j}(x,y)}$*, where* $\underline{j}(x, y)$ *is the smallest integer* j *such that* $x_0^j \le x \le x_1^j$ *and* $y_0^j \le y \le y_1^j$*.*

Parameter	x_0^j	x_1^j	y_0^j	y_1^j	True value
θ_1	.6	1	.15	.3	-1
θ_2	.2	.35	0	.3	1.3
θ_3	.5	1	0	.5	-1.4
θ_4	.4	1	.6	1	2.7
θ_5	0.0	0.4	.7	1	-1
θ_6	0.0	1.0	0.0	1.0	-3

Modeling tracer evolution requires first computing the hydraulic head, which determines the groundwater velocity. Under the Dupuit approximation [17], the hydraulic head h obeys the elliptic equation,

$$\nabla \cdot (\kappa h \nabla h) = -f_h, \tag{5.6}$$

where $\kappa(x, y)$ is the conductivity field and $f_h(x, y)$ is the hydraulic head forcing. In our problem setup, the forcing is created by pumping at four well locations, $(a_i, b_i) \in \{(0.15, 0.15), (0.85, 0.15), (0.85, 0.85), (0.15, 0.85)\}$, such that

$$f_h(x, y) = \sum_{i=1}^{4} 2.0 \exp\left(\frac{(a_i - x)^2 + (b_i - y)^2}{.02}\right).$$

The model (5.6) assumes homogeneous Dirichlet boundary conditions at $y = 0$ and $y = 1$ and homogeneous Neumann conditions at $x = 0$ and $x = 1$. The Darcy velocity is

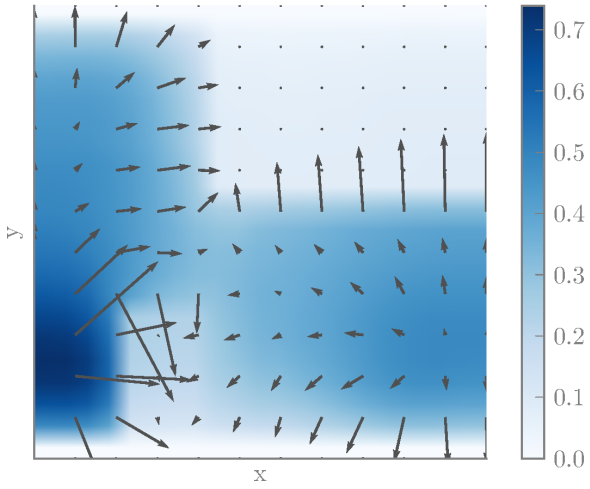

Figure 5.3. *Hydraulic head (shading) $h(x, y)$ computed via (5.6) and corresponding velocities (5.7), given the conductivity field in Figure 5.2.*

determined by the hydraulic head gradient

$$\begin{bmatrix} u \\ v \end{bmatrix} = -h\kappa\nabla h. \tag{5.7}$$

The time-dependent tracer concentration $c(x, y, t)$ then evolves given a flow-dependent dispersion tensor

$$\frac{\partial c}{\partial t} + \nabla \cdot \left(\left(d_m \mathbf{I} + d_l \begin{bmatrix} u^2 & uv \\ uv & v^2 \end{bmatrix} \right) \nabla c \right) - \begin{bmatrix} u \\ v \end{bmatrix} \cdot \nabla c = -f_t, \tag{5.8}$$

where $d_m = 5 \times 10^{-3}$ and $d_l = 5 \times 10^{-4}$ are dispersion coefficients and $f_t(x, y)$ is the tracer forcing. The tracer is forced by injection at the two leftmost well locations, $(a_i, b_i) \in \{(0.15, 0.15), (0.15, 0.85)\}$, expressed via a source term of similar form,

$$f_t(x, y) = \sum_{i=1}^{2} 15.0 \exp\left(\frac{(a_i - x)^2 + (b_i - y)^2}{.02} \right).$$

The tracer has initial condition $c(x, y, 0) = 0$, and homogeneous Neumann conditions are enforced at all spatial boundaries. Since the hydraulic head forcing, tracer forcing, and dispersion coefficients are known, the forward model simply maps the conductivity to a time-evolving concentration field. Tracer observations are taken at nine well locations $\{(x_i, y_i) \in \{((.15, .15), (.15, .5), (.15, .85), (.5, .15), (.5, .5), (.5, .85), (.85, .15), (.85, .5), (.85, .85)\}$ at successive times $t \in \{1, 2, 3, 4, 5\}$.

The forward solver computes the steady state pressure and velocity fields, then simulates the tracer advection/diffusion, which takes several seconds of computation. Figure 5.3 shows the pressure and velocity fields resulting from the true log-conductivity, and Figure 5.4 shows the associated tracer concentration field at $t = 3$. Data for inversion are generated using a standard finite element scheme on a 25×25 mesh. The solver used for inversion (i.e., to

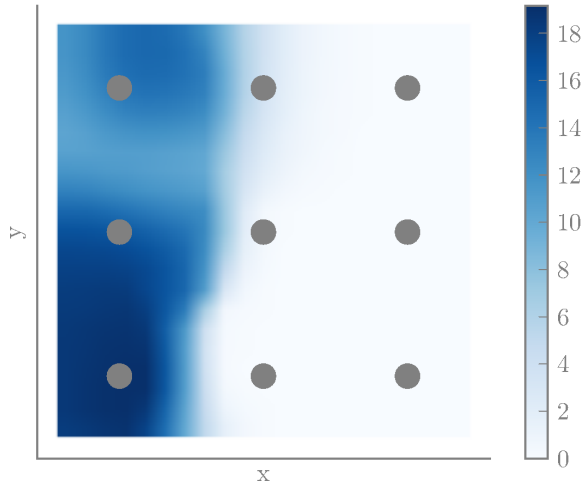

Figure 5.4. *The tracer concentration at the middle observation time, $c(x, y, t = 3)$, given the conductivity field in Figure 5.2. The tracer is introduced at the top-left and bottom-left wells. All the well locations are shown by overlaid dots.*

evaluate the posterior density at a candidate value of θ) uses a coarser 12×12 mesh. The likelihood assumes additive and i.i.d. errors for each observation of tracer concentration, Gaussian with mean zero and variance 10^{-4}.

The posterior distribution in this problem has no standard analytical form. To establish a baseline for accuracy comparisons, we instead run ten "reference" chains that employ no approximation of the forward model. Each chain is simulated using 10^5 steps of adaptive Metropolis (AM) [22] which requires several days (per chain) of computation. After discarding the first 10^4 samples of each chain as burn-in, the remaining samples are pooled and used to characterize the posterior distribution. One- and two-dimensional marginals of the posterior are shown in Figure 5.5. The distribution has distinctly non-Gaussian structures.

Next, we run the single-chain local approximation algorithm, using quadratic approximations of the forward model coupled with AM or with mMALA, and setting the refinement parameters to $\beta_t = 0.01t^{-0.2}$ and $\gamma_t = 0.1t^{-0.1}$ (see Appendix A). For each type of proposal, we run ten independent chains of 10^5 samples and discard the first 10^4 samples of each chain as burn-in. The convergence of these chains as a function of wall clock time is shown in Figure 5.6. Here, the vertical axis depicts a relative error in multiple posterior moments, computed as the chain evolves: in particular, we estimate the posterior covariance using MCMC samples (after burn-in), compare this estimate to the reference covariance estimate by taking the Frobenius norm of the difference, and then normalize by the Frobenius norm of the reference covariance. The AM experiments exhibit accuracy comparable to the reference chains, but with a wall clock time that is about fifty times shorter—less than an hour per chain. mMALA is more expensive than AM, but appears to provide more accurate chains; the error in posterior covariance estimates drops more quickly, reflecting better mixing. A plausible explanation for the increased computational cost of mMALA (over AM) is that the cross-validation error indicator, applied to the Metropolis acceptance probability, is more sensitive to errors in the approximation when the proposal distribution relies on gradients thereof. Overall, though, mMALA with local approximations is still significantly cheaper

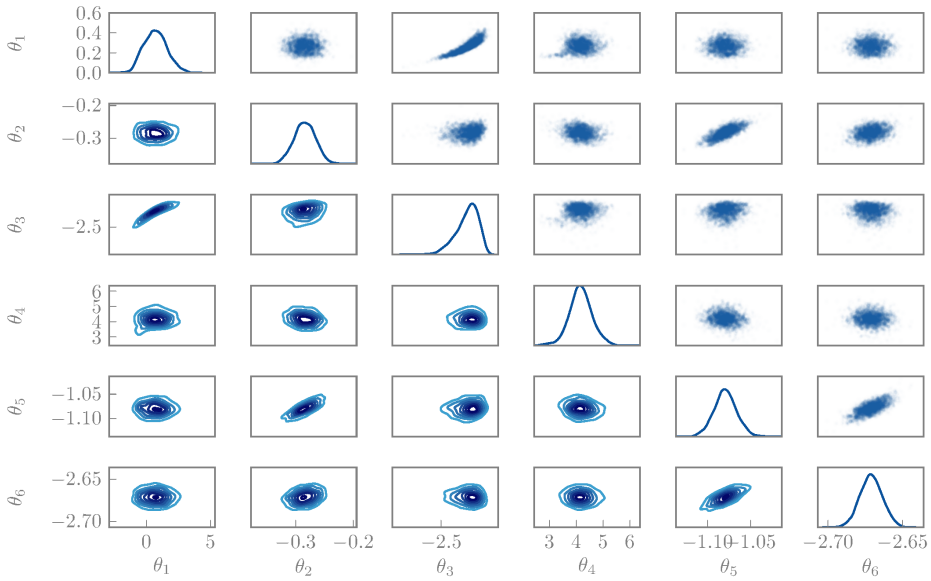

Figure 5.5. *One- and two-dimensional posterior marginals of the parameters in the hydrologic tracer transport problem.*

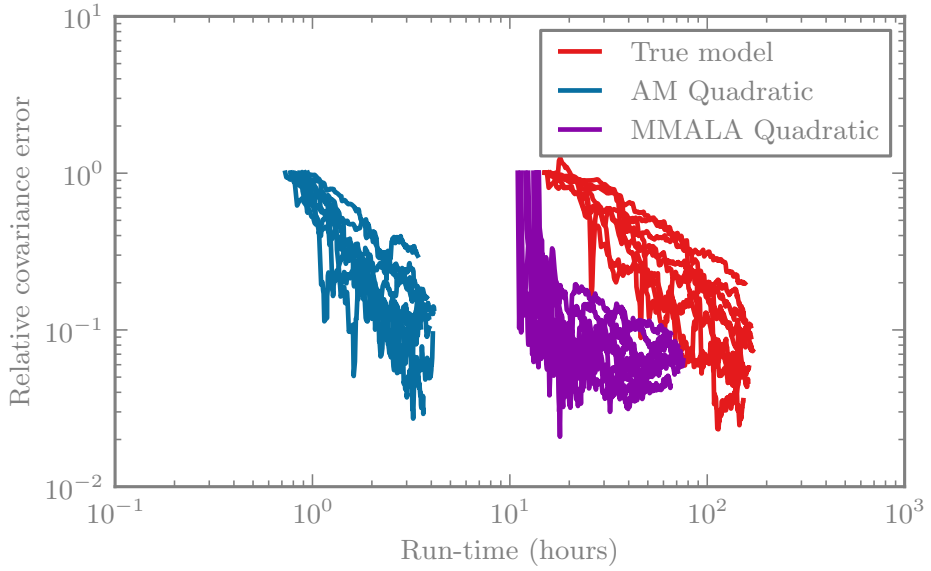

Figure 5.6. *Relative error in the posterior covariance for serial runs of MCMC on the tracer transport problem, using the true model and quadratic approximations coupled with different proposal schemes. The plot depicts ten independent chains of each type, with the first 10% of each chain removed as burn-in.*

than running AM on the true model.

Having the established the accuracy of the approximate chains, we now investigate the efficiency of the sampler in a parallel setting. To do so, we estimate the effective sample size (ESS) produced by the chains as a function of computational effort. For all cases, we hold the length of each MCMC chain fixed at 10^5 samples and discard the initial 10% of every

chain when estimating ESS, but include the computational cost of the discarded portion.

We make two comparisons. First, Figure 5.7 shows the total number of effectively independent samples produced across parallel chains, as a function of wall clock time. Each level of shading (from dark to light) corresponds to an increased number of parallel chains, as indicated in the figure legend. Blue dots represent runs with AM proposals and purple dots represent mMALA runs. The red dots represent single MCMC chains simulated without any approximation; these serve as a lower bound on ESS and an upper bound on computational time. We obviously expect parallel chains to produce a larger ESS once their samples are pooled, and indeed the dots move upwards as the number of concurrent chains is increased. But the dots representing AM and mMALA also move to the left; in other words, parallel experiments actually complete *more quickly* because of their collaboration. Additionally, mMALA yields higher ESS than AM both in the single-chain case and at a comparable level of parallelism (10 chains), suggesting that it does indeed mix more effectively.

Our second comparison uses a more stringent measure of parallel efficiency: ESS per CPU–second,[2] which removes the intrinsic advantage of having multiple chains. A naïve MCMC parallelization would yield no improvement in efficiency according to this metric: the number of samples might grow linearly with the number of chains, but this growth would be normalized away. In contrast, results using our parallel algorithm, shown in Figure 5.8, show steady gains in ESS/(CPU–second) with additional parallel workers. This gain is the result of collaboration among the chains in the most computationally costly element of the algorithm—running the forward model $\mathbf{f}$—via the shared and asynchronous construction of the evaluation set $\mathcal{S}_t$, from which each chain can construct local approximations. Note that additional parallel chains are not computed "for free"; the total number of model evaluations performed during the parallel experiments is still higher than in the single-chain case. But gains in efficiency mean that larger ESS values more than offset this computational cost. We also note that while mMALA chains yield a larger total ESS, they are less efficient in the ESS/(CPU–second) metric for this problem. That said, the performance gap is sufficiently small that one could expect mMALA to outperform AM in problems where MCMC mixing is more difficult, and hence where locally adapted proposals are needed.

5.2. Shallow-shelf ice stream model. Continental ice sheets are divided into basins that are drained by fast-flowing river-like ice streams. These ice streams regulate the discharge of ice mass into the ocean, and hence play a key role determining the overall behavior of the ice sheet. The IPCC has identified the Antarctic contribution to sea-level rise as an important source of uncertainty in climate projections, and ice streams have become a widespread topic of study [2, 23].

Ice stream dynamics are not completely understood, nor are the factors governing their dynamics. Although satellite data provide plentiful observations of topology and surface velocities [19, 28, 44], basal properties, such as the friction between the base of the ice and the underlying ground—the *basal friction*—are difficult or impossible to observe directly. The basal friction varies widely, and may be higher if the ice is scraping directly against rough bedrock or lower if the ice rests on till, a mixture of mud and rock that lubricates the interface. The basal friction also parameterizes basal lubrication caused by melting basal ice (possibly due to geothermal or frictional heating). Previous work infers basal friction given

[2] We use one chain per CPU.

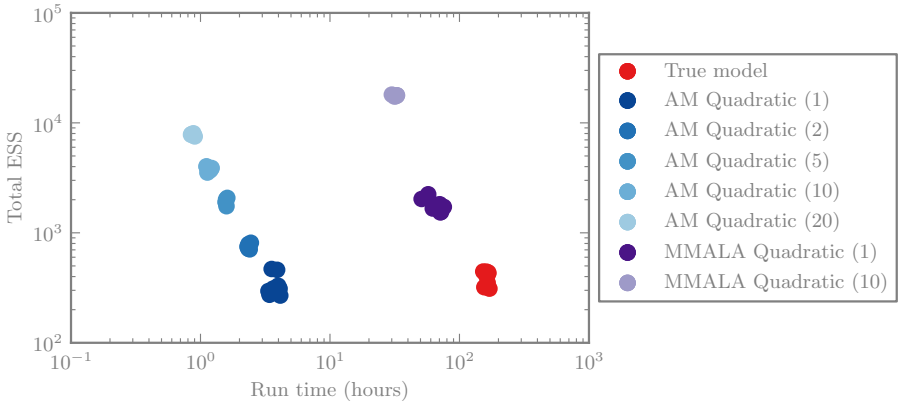

Figure 5.7. *Results of the parallel efficiency study on the tracer transport problem, comparing run time to the total effective sample size (ESS) across all parallel chains. Each dot represents one (parallel) experiment. The number in parentheses corresponds to the number of parallel chains used in each experiment. Using more chains increases ESS* and *decreases run time.*

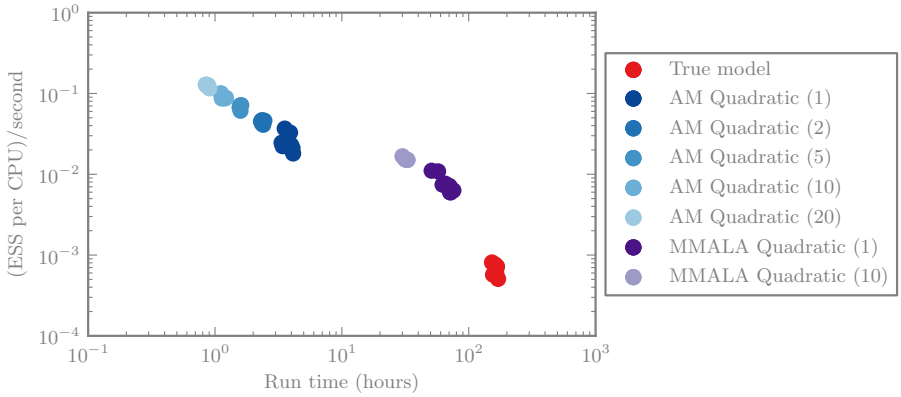

Figure 5.8. *Results of the parallel efficiency study on the tracer transport problem, comparing run time to the effective number of samples produced per CPU–second. Each dot represents one (parallel) experiment. Again, the number in parentheses corresponds to the number of parallel chains used in each experiment.*

surface velocity observations [30, 37]; quantifying uncertainty in the basal friction, however, requires considerable computational expense and/or posterior approximations [36]. In this example, we explore the problem of inferring the basal friction from surface velocities, employing local approximations to reduce the computational cost of MCMC.

Ice is often modeled as a highly, viscous non-Newtonian, and incompressible fluid. In particular, the shallow-shelf approximation [29, 30, 31] describes ice stream velocity assuming that *(i)* the horizontal extent ($\mathcal{O}(100\,\mathrm{km})$) is much larger than the vertical extent ($\mathcal{O}(1\,\mathrm{km})$); and *(ii)* the vertical velocity is zero. The nondimensionalized shallow shelf

equations for a two-dimensional horizontal domain $[0,1]^2 \ni (x,y)$ are

$$\frac{\partial}{\partial x}\left(2\nu h\left(2\frac{\partial u}{\partial x}+\frac{\partial v}{\partial y}\right)\right)+\frac{\partial}{\partial y}\left(\nu h\left(\frac{\partial u}{\partial y}+\frac{\partial v}{\partial x}\right)\right)-\beta\left|u\right|^{m-1}u=h\frac{\partial s}{\partial x}$$
$$\frac{\partial}{\partial x}\left(2\nu h\left(2\frac{\partial v}{\partial y}+\frac{\partial u}{\partial x}\right)\right)+\frac{\partial}{\partial y}\left(\nu h\left(\frac{\partial v}{\partial x}+\frac{\partial u}{\partial y}\right)\right)-\beta\left|v\right|^{m-1}v=h\frac{\partial s}{\partial y},$$

with boundary conditions

$$u=0 \quad \text{and} \quad v=-1 \quad \text{at} \quad x=0 \quad \text{and} \quad x=1,$$
$$\tfrac{\partial u}{\partial y}+\tfrac{\partial v}{\partial x}=0 \quad \text{at} \quad y=0 \quad \text{and} \quad y=1, \text{and} \quad 2\tfrac{\partial v}{\partial y}+\tfrac{\partial u}{\partial x}=0 \quad \text{at} \quad y=1,$$

where

$$\nu=\frac{1}{2}\left(\left(\frac{\partial u}{\partial x}\right)^2+\left(\frac{\partial v}{\partial y}\right)^2+\frac{1}{4}\left(\frac{\partial u}{\partial y}+\frac{\partial v}{\partial x}\right)^2+\frac{\partial u}{\partial x}\frac{\partial v}{\partial y}\right)^{-\frac{n-1}{2n}}$$

is the velocity-dependent viscosity [29, 30, 31]. Assuming that the surface elevation $s(x,y)$ and ice thickness $h(x,y)$ are known and that $n=\frac{1}{m}=3$, the forward model maps realizations of the basal friction $\beta(x,y)$ to the horizontal velocities $u(x,y)$ and $v(x,y)$.

To define our Bayesian inference problem, we endow the log-basal friction field $\log\beta(x,y)$ with a Gaussian process prior, using an isotropic squared-exponential covariance kernel,

$$C\left((x_1,y_1),(x_2,y_2)\right)=\sigma^2\exp\left(-\frac{(x_1-x_2)^2+(y_1-y_2)^2}{2l^2}\right),$$

with correlation length $l=0.1$ and variance $\sigma^2=25$. This field is easily parameterized with a Karhunen-Loève (K-L) expansion [1]:

$$\beta(x,y;\theta)\approx\exp\left(\sum_{i=1}^{d}\theta_i\sqrt{\lambda_i}\varphi_i(x,y)\right),$$

where λ_i and $\varphi_i(x,y)$ are the eigenvalues and eigenfunctions, respectively, of the integral operator on $[0,1]^2$ defined by the kernel C, and the parameters θ_i inherit independent standard normal priors, $\theta_i\sim\mathcal{N}(0,1)$. We truncate the Karhunen-Loève expansion at $d=12$ modes and infer the weights $(\theta_1,\ldots,\theta_{12})$ from data. The true basal diffusivity field is shown in Figure 5.9.

Data arise from observations of the velocity field on a uniform 10×10 grid covering the unit square, $(x_i,y_i)\in\{(.05,.05),\ldots,(.95,.95)\}$, as depicted in Figure 5.10. Both the u and v components of velocity are observed, and observational errors are taken to be independent, additive, and identically Gaussian, $\mathcal{N}(0,0.01^2)$. To avoid an "inverse crime," data are generated with a 25×25 mesh but inference uses a coarser 15×15 mesh.

The posterior distribution of the basal friction field is quite challenging to sample, as the forward model requires, on average, 26 seconds per evaluation. Using a direct MCMC approach, a numerical simulation comprising 10 parallel chains of 200,000 steps each would therefore take nearly two months to run. Using AM with quadratic approximations, we

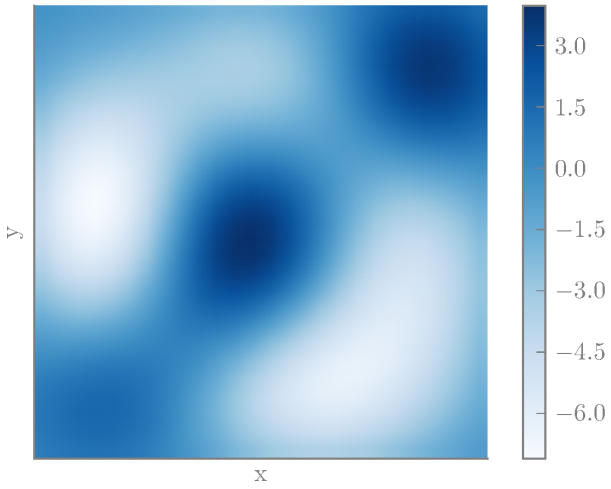

Figure 5.9. *Ice stream inference problem: the true log-basal friction field,* $\log \beta(x, y)$.

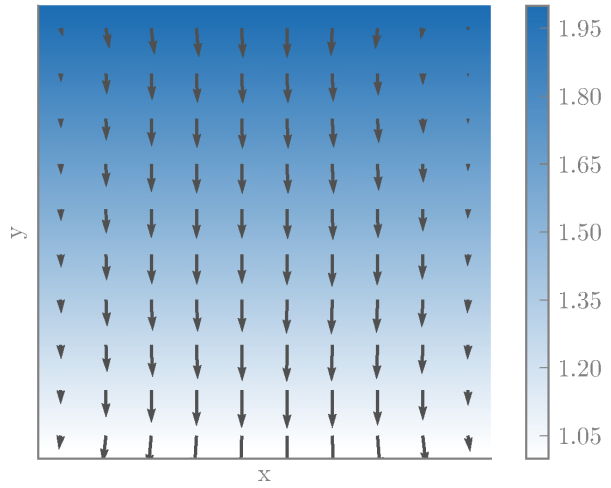

Figure 5.10. *Ice stream inference problem: the assumed ice height field* $h(x, y)$ *(shading) superimposed on the observed velocity field (vectors), given the basal friction in Figure 5.9. Note the left–right asymmetry in the velocity field at the top of the domain, induced by the high friction region at the top right.*

complete exactly the same simulation in just over one day, a nearly 60-fold improvement in the run time. Representative one- and two-dimensional marginals of the posterior (focussing on only the first 6 of 12 dimensions) are shown in Figure 5.11. Note that several parameters are strongly correlated, and that many marginal distributions appear skewed and non-Gaussian. These two million samples were produced using only about 35,000 runs of the forward model.

6. Conclusions. This work has extended our previous development of asymptotically exact MCMC algorithms that employ local approximations of expensive models. We lifted restrictive assumptions on the type of MCMC kernel that could be used—in particular, allowing the proposal distribution to extract derivatives, and hence geometric information, from the approximation. Doing so enables a wide variety of more sophisticated proposal

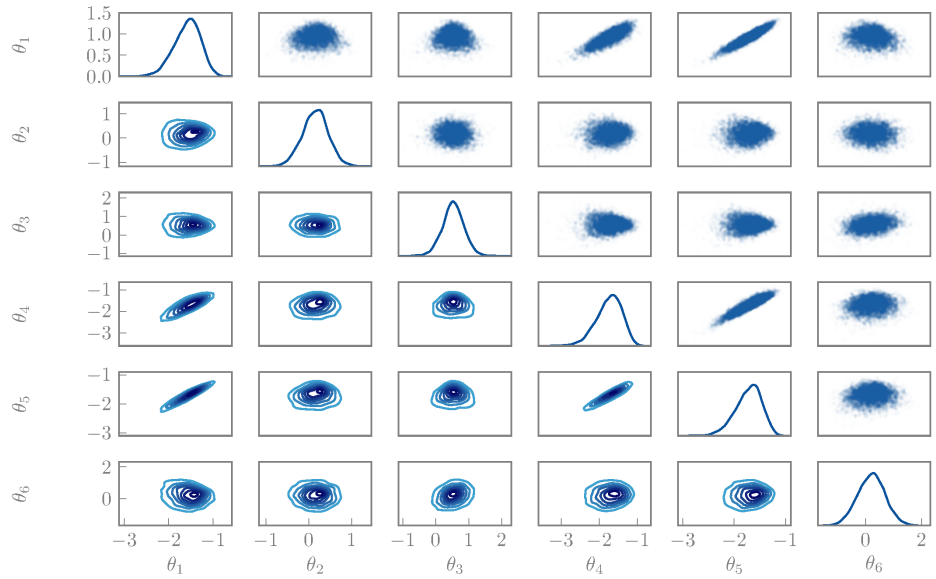

Figure 5.11. *One- and two-dimensional posterior marginals of the first six parameters in the ice stream inference problem.*

distributions, such as manifold MALA, to be applied in settings where they would otherwise be intractable (e.g., when forward model derivatives cannot be directly evaluated) or unaffordable. Additionally, we showed that using approximations allows the most computational intensive element of many MCMC simulations—the forward model or likelihood evaluations—to be directly parallelized, through the shared and online construction of a posterior-adapted set of samples. Sharing this set of model evaluations among multiple MCMC chains drives the construction of local approximations on each chain, providing a novel and effective means of reducing the run time of MCMC simulations.

To demonstrate the practical utility of these developments, we presented two challenging benchmark problems that we believe reflect scientifically interesting problems where forward models are necessarily expensive. Using parallel computing resources, we demonstrated a greater than two-order-of-magnitude improvement in the run time of a groundwater hydrology inference problem, and a nearly 60-fold reduction in the run time of an ice stream inference problem. These results suggest that our approach may help make a range of challenging Bayesian inference problems feasible. A reusable and open source implementation of this algorithm is available as part of the MIT Uncertainty Quantification Library, http://muq.mit.edu.

Acknowledgments. This work was supported in part by the Scientific Discovery through Advanced Computing (SciDAC) program of the US Department of Energy, Office of Science, Advanced Scientific Computing Research under award number DE-SC0007099 (P. Conrad, A. Davis, and Y. Marzouk), by the National Sciences and Engineering Research Council of Canada (A. Smith), and by the Office of Naval Research (N. Pillai).

Appendix A. Complete algorithm description. This appendix provides a complete description of the local approximation MCMC algorithm from [10], here extended to MCMC

proposals that also employ the approximation $\tilde{\mathbf{f}}$. We replicate necessary subroutines from [10]; for a full discussion and derivation of these methods, please see that paper. The sketch given in Algorithm 4.2 of Section 2 is here expanded into Algorithm A.3, which takes additional parameters β_t and γ_t that determine when refinement is performed according to random or cross validation criteria, respectively. The choice of γ_t is arbitrary, but $\sum \beta_t$ must diverge; based on the parameter study in [10], the numerical experiments in Section 5 are performed with $\beta_t = 0.01t^{-0.2}$ and $\gamma_t = 0.1t^{-0.1}$.

Algorithm A.3 Metropolis-Hastings with local approximations and general proposals

1: **procedure** RunChain($\mathbf{f}, r, \theta_1, \mathcal{S}_1, \ell, \mathbf{d}, p, T, \{\beta_t\}_{t=1}^T, \{\gamma_t\}_{t=1}^T$)
2: **for** $t = 1 \dots T$ **do**
3: $(\theta_{t+1}, \mathcal{S}_{t+1}) \leftarrow K_t(\theta_t, \mathcal{S}_t, \ell, \mathbf{d}, p, \mathbf{f}, r, q, \beta_t, \gamma_t)$
4: **end for**
5: **end procedure**

6: **procedure** $K_t(\theta^-, \mathcal{S}, \ell, \mathbf{d}, p, \mathbf{f}, r, q, \beta_t, \gamma_t)$
7: Draw proposal $\mathbf{z}_t \sim \mathcal{N}(0, I)$
8: $\tilde{\mathbf{f}}^- \leftarrow$ LocApprox$(\theta^-, \mathcal{S}, \emptyset)$
9: $\theta^+ \leftarrow r(\theta^-, \mathbf{z}, \tilde{\mathbf{f}}^-)$
10: $\tilde{\mathbf{f}}^+ \leftarrow$ LocApprox$(\theta^+, \mathcal{S}, \emptyset)$
11: $\alpha \leftarrow \min\left(1, \frac{\ell(\theta^+|\mathbf{d}, \tilde{\mathbf{f}}^+) p(\theta^+) q(\theta^+, \theta^-|\tilde{\mathbf{f}}^+)}{\ell(\theta^-|\mathbf{d}, \tilde{\mathbf{f}}^-) p(\theta^-) q(\theta^-, \theta^+|\tilde{\mathbf{f}}^-)}\right)$ ▷ Compute nominal acceptance ratio
12: Compute ϵ^+ and ϵ^- as in (A.9)–(A.10).
13: **if** $u \sim \text{Uniform}(0,1) < \beta_m$ **then** ▷ Refine with probability β_m
14: Randomly, $\mathcal{S} \leftarrow$ RefineNear$(\theta^+, \mathcal{S})$ or $\mathcal{S} \leftarrow$ RefineNear$(\theta^-, \mathcal{S})$
15: **else if** $\epsilon^+ \geq \epsilon^-$ and $\epsilon^+ \geq \gamma_m$ **then** ▷ If needed, refine near the larger error
16: $\mathcal{S} \leftarrow$ RefineNear$(\theta^+, \mathcal{S})$
17: **else if** $\epsilon^- > \epsilon^+$ and $\epsilon^- \geq \gamma_m$ **then**
18: $\mathcal{S} \leftarrow$ RefineNear$(\theta^-, \mathcal{S})$
19: **end if**
20: **if** refinement occurred **then** repeat from Line 8.
21: **else** ▷ Evolve chain using approximations
22: Draw $u \sim \text{Uniform}(0,1)$. If $u < \alpha$, **return** $(\theta^+, \mathcal{S})$, else **return** $(\theta^-, \mathcal{S})$.
23: **end if**
24: **end procedure**

Algorithm A.4 provides several subroutines. The first, LocApprox, gathers the N nearest neighbors from $\mathcal{S}_t$ to use in constructing the approximation; for quadratics, $N = \frac{\sqrt{d}(d+1)(d+2)}{2}$. The operator $\mathcal{A}^{\sim j}_{\mathcal{B}(\theta,R)}$ constructs the local approximation; in this work, it fits a quadratic (a degree-two polynomial) with least squares. The input j facilitates cross validation and unless $j = \emptyset$, designates that the jth neighbor should be omitted. The second routine, RefineNear, solves a local optimization problem to choose a new point θ^* that is near θ but space-filling overall; this point is used to enrich $\mathcal{S}_t$.

Cross validation is used to estimate the error in the acceptance probability evaluated using the approximations. Define the nominal and leave-one-out variants of the approxi-

Algorithm A.4 Supporting algorithms

procedure LocApprox($\theta, \mathcal{S}, j$)
  Select R so that $|\mathcal{B}(\theta, R)| = N$, where $\mathcal{B}(\theta, R) := \{(\theta_i, \mathbf{f}(\theta_i)) \in \mathcal{S} : \|\theta_i - \theta\|_2 \le R\}$ ▷ Select ball of points
  $\tilde{\mathbf{f}} \leftarrow \mathcal{A}^{\sim j}_{\mathcal{B}(\theta,R)}$ ▷ Fit local approximation
  return $\tilde{\mathbf{f}}$
end procedure

procedure RefineNear($\theta, \mathcal{S}$)
  Select R so that $|\mathcal{B}(\theta, R)| = N$ ▷ Select ball of points
  $\theta^* \leftarrow \arg\max_{\|\theta'-\theta\| \le R} \min_{\theta_i \in \mathcal{S}} \|\theta' - \theta_i\|$ ▷ Optimize near θ
  $\mathcal{S} \leftarrow \mathcal{S} \cup \{\theta^*, \mathbf{f}(\theta^*)\}$ ▷ Grow the sample set
  return $\mathcal{S}$
end procedure

mations, for $j = 1, \ldots, N$, as

$$\tilde{\mathbf{f}}^+ = \text{LocApprox}(\theta^+, \mathcal{S}, \emptyset) \qquad \tilde{\mathbf{f}}^+_{\sim_j} = \text{LocApprox}(\theta^+, \mathcal{S}, j)$$
$$\tilde{\mathbf{f}}^- = \text{LocApprox}(\theta^-, \mathcal{S}, \emptyset) \qquad \tilde{\mathbf{f}}^-_{\sim_j} = \text{LocApprox}(\theta^-, \mathcal{S}, j).$$

Then compute the approximate posterior ratio and all the leave-one-out variants (here slightly modified from our original work to include the proposal densities),

$$\zeta := \frac{\ell(\theta^+|\mathbf{d}, \tilde{\mathbf{f}}^+)p(\theta^+)q(\theta^+, \theta^-|\tilde{\mathbf{f}}^+)}{\ell(\theta^-|\mathbf{d}, \tilde{\mathbf{f}}^-)p(\theta^-)q(\theta^-, \theta^+|\tilde{\mathbf{f}}^-)}$$
$$\zeta^{+,\sim j} := \frac{\ell(\theta^+|\mathbf{d}, \tilde{\mathbf{f}}^+_{\sim_j})p(\theta^+)q(\theta^+, \theta^-|\tilde{\mathbf{f}}^+_{\sim_j})}{\ell(\theta^-|\mathbf{d}, \tilde{\mathbf{f}}^-)p(\theta^-)q(\theta^-, \theta^+|\tilde{\mathbf{f}}^-)}$$
$$\zeta^{-,\sim j} := \frac{\ell(\theta^+|\mathbf{d}, \tilde{\mathbf{f}}^+)p(\theta^+)q(\theta^+, \theta^-|\tilde{\mathbf{f}}^+)}{\ell(\theta^-|\mathbf{d}, \tilde{\mathbf{f}}^-_{\sim_j})p(\theta^-)q(\theta^-, \theta^+|\tilde{\mathbf{f}}^-_{\sim_j})}$$

Finally, find the maximum difference between the α values computed using ζ and those computed using the leave-one-out variants $\zeta^{+,\sim j}$ and $\zeta^{-,\sim j}$, averaging over the forward and reverse directions. These are the error indicators:

$$\epsilon^+ := \max_j \left(\left| \min(1, \zeta) - \min\left(1, \zeta^{+,\sim j}\right) \right| + \left| \min\left(1, \frac{1}{\zeta}\right) - \min\left(1, \frac{1}{\zeta^{+,\sim j}}\right) \right| \right) \tag{A.9}$$

$$\epsilon^- := \max_j \left(\left| \min(1, \zeta) - \min\left(1, \zeta^{-,\sim j}\right) \right| + \left| \min\left(1, \frac{1}{\zeta}\right) - \min\left(1, \frac{1}{\zeta^{-,\sim j}}\right) \right| \right). \tag{A.10}$$

Appendix B. Proofs of the main results. Throughout this section, we use the notation $f(x) = O(g(x))$ to mean that there exists some constant $0 < C < \infty$ so that $f(x) \le Cg(x)$. If the constant C depends on an important parameter, we sometimes use that parameter as a subscript for emphasis; for example, $\frac{x^2}{p} = O_p(x^4)$ for all fixed $p > 0$, but there is no constant $C < \infty$ so that $\frac{x^2}{p} \le Cx^4$ uniformly in $p > 0$.

For any pair of measures μ, ν on a metric space $(\mathcal{X}, d)$, denote by $\Pi(\mu, \nu)$ the collection of all pairs of random variables $(X, Y) \in \mathcal{X}^2$ that have marginal distributions $\mathcal{L}(X) = \mu$, $\mathcal{L}(Y) = \nu$. Recall that the *Wasserstein metric* on measures on a metric space $(\mathcal{X}, d)$ is given by

$$W_d(\mu, \nu) = \inf_{(X,Y)\in\Pi(\mu,\nu)} \mathbb{E}[d(X, Y)].$$

We also use the shorthand $W_p \equiv W_{\|\cdot\|_p}$ when $1 \leq p \leq \infty$. The *total variation* distance between two probability measures μ, ν is given by $\|\mu - \nu\|_{\mathrm{TV}} = W_\rho(\mu, \nu)$, where $\rho(x, y) \equiv \mathbf{1}_{x\neq y}$. The *mixing time* of a Markov chain $\{Z_t\}_{t\geq 0}$ with stationary distribution π on state space Ω is

$$\tau_{\mathrm{mix}} = \inf\{t : \sup_{Z_0=z\in\Omega} \|\mathcal{L}(Z_t) - \pi\|_{\mathrm{TV}} < \frac{1}{4}\}.$$

Proof of Theorem 4.6. Denote the diameter of Ω by D_Ω and the mixing time of K_∞ by τ_{mix}; by parts 1 and 2 of Assumption 3.1, respectively, $D_\Omega, \tau_{\mathrm{mix}} < \infty$. For $\epsilon > 0$, let $\tau_\epsilon = \inf\{t > 0 : \mathcal{S}_t \text{ is an } \epsilon - \text{cover of } \Theta\}$. By substituting τ_ϵ for τ everywhere that it is used, the proof of Lemma B.4 of [10] shows that

$$\mathbb{P}[\tau_\epsilon < \infty] = 1 \tag{B.11}$$

for all $\epsilon > 0$.

Next, fix $S, T \in \mathbb{N}$ and $\psi, \delta, \varphi_0 > 0$, and let $\epsilon = \epsilon(\delta)$ be the smaller of the values of $\epsilon(\delta)$ from inequalities (4.2), (4.4). Let $\mathcal{F}_T$ be the σ-algebra $\sigma(\{X_t, \mathcal{S}_t\}_{0\leq t\leq T})$. We will let $\{Y_t\}_{t\geq T}$ be a Markov chain with transition kernel K_∞ started at $Y_T = X_T$ and we will let $\{Z_t\}_{t\geq T}$ be a Markov chain with transition kernel K_∞ started at the distribution $\mathcal{L}(Z_T) = \pi$. We now describe a coupling of the three stochastic processes $\{X_t\}_{T\leq t\leq T+S}$, $\{Y_t\}_{T\leq t\leq T+S}$, and $\{Z_t\}_{T\leq t\leq T+S}$. We couple $\{Y_t\}_{T\leq t\leq T+S}$, $\{Z_t\}_{T\leq t\leq T+S}$ so that

$$\mathbb{P}[Y_{T+S} = Z_{T+S}|Y_T, Z_T] = \|\mathcal{L}(Y_{T+S}|Y_T) - \mathcal{L}(Z_{T+S}|Z_T)\|_{\mathrm{TV}}. \tag{B.12}$$

At least one coupling with this property exists by the definition of the total variation distance; choose one such coupling arbitrarily. We then couple $\{X_t\}_{T\leq t\leq T+S}$ to $\{Y_t\}_{T\leq t\leq T+S}$ iteratively in t. Denote by $\tilde{X}$ the value that would be returned in the (t)th iteration of Algorithm A.3 if Step 21 were ignored, and let $\mathbf{z}$ be the value obtained in Step 7. Then, (X_{t+1}, Y_{t+1}) can be coupled conditional on $(X_t, Y_t, \mathcal{S}_t)$ so that

$$\begin{aligned}\mathbb{E}[\|X_{t+1} - Y_{t+1}\|_2] \leq& \mathbb{E}[\|X_{t+1} - \tilde{X}\|] + \mathbb{E}[\|\tilde{X} - Y_{t+1}\|] \leq \delta + D_\Omega \mathbb{P}[\|\mathbf{z}\| > \varphi_0] + \frac{\psi}{S+1} \\ &+ \sup_{\theta,\theta'\in\Theta,\, \|\theta-\theta'\|<\|X_t-Y_t\|} W_2(K_{\mathcal{S}_t}(\theta, \cdot), K_\infty(\theta', \cdot)).\end{aligned} \tag{B.13}$$

Such a coupling exists by inequality (4.4) and the definition of the Wasserstein distance. By the 'gluing' lemma (Chapter 1 of [46]), it is possible to combine the couplings of $\{X_t, Y_t\}_{T\leq t\leq T+S}$ and $\{Y_t, Z_t\}_{T\leq t\leq T+S}$ into a single coupling $\{X_t, Y_t, Z_t\}_{T\leq t\leq T+S}$ that satisfies both inequality (B.12) and also inequality (B.13) for all $T \leq t < T + S$. Under this coupling,

$$W_2(Y_{T+S}, Z_{T+S}) \leq D_\Omega \mathbb{P}[Z_{T+S} \neq Y_{T+S}] \tag{B.14}$$

$$\leq D_\Omega 2^{-\lfloor \frac{S}{\tau_{\text{mix}}} \rfloor}.$$

Let η_0 be as in the requirements for (4.3). By inequalities (4.2) and (B.13), we have for $T \leq t < T+S$ that

$$\begin{aligned}
\mathbb{E}[\|X_{t+1} - Y_{t+1}\|_2 \,|\mathcal{F}_T] &= \mathbb{E}[\|X_{t+1} - Y_{t+1}\|_2 \mathbf{1}_{T \geq \tau_\epsilon} |\mathcal{F}_T] + \mathbb{E}[\|X_{t+1} - Y_{t+1}\|_2 \mathbf{1}_{T < \tau_\epsilon} |\mathcal{F}_T] \\
&\leq \delta + D_\Omega \mathbb{P}[\|\mathbf{z}\| > \varphi_0] + \frac{\psi}{S+1} + \mathbb{E}[\sup_{\theta, \theta' \in \Theta,\, \|\theta - \theta'\| < \|X_t - Y_t\|} W_2(K_\infty(\theta, \cdot), K_\infty(\theta', \cdot)) | \mathcal{F}_T] \\
&+ \mathbb{E}[\sup_{\theta \in \Theta} W_2(K_{\mathcal{S}_t}(\theta, \cdot), K_\infty(\theta, \cdot)) \mathbf{1}_{T \geq \tau_\epsilon} |\mathcal{F}_T] + D_\Omega \mathbf{1}_{T < \tau_\epsilon} \\
&\leq \delta + D_\Omega \mathbb{P}[\|\mathbf{z}\| > \varphi_0] + \frac{\psi}{S+1} + C\mathbb{E}[\|X_t - Y_t\|_2 \,|\mathcal{F}_T] + D_\Omega \mathbb{P}[\|X_t - Y_t\| \geq \eta_0 | \mathcal{F}_T] \\
&+ \delta + D_\Omega \mathbf{1}_{T < \tau_\epsilon} \\
&\leq D_\Omega \mathbb{P}[\|\mathbf{z}\| > \varphi_0] + \frac{\psi}{S+1} + 2\delta + (C + \frac{D_\Omega}{\eta_0}) \mathbb{E}[\|X_t - Y_t\|_2 \,|\mathcal{F}_T] + D_\Omega \mathbf{1}_{T < \tau_\epsilon}.
\end{aligned}$$

Iterating this inequality over $T \leq t < T+S$ and recalling that $\|X_T - Y_T\|_2 = 0$,

$$\begin{aligned}
\text{(B.15)} \quad \mathbb{E}[\|X_{T+S} - Y_{T+S}\|_2 \,|\mathcal{F}_T] &\leq (2\delta + \frac{\psi}{S+1} + D_\Omega \mathbb{P}[\|\mathbf{z}\| > \varphi_0])(C + \frac{D_\Omega}{\eta_0})^{S+1} \\
&+ D_\Omega \mathbf{1}_{T < \tau_\epsilon}.
\end{aligned}$$

Combining inequalities (B.14) and (B.15),

$$\begin{aligned}
W_2(X_{T+S}, \pi) &\leq \mathbb{E}[\|X_{T+S} - Z_{T+S}\|_2] \\
&\leq D_\Omega 2^{-\lfloor \frac{S}{\tau_{\text{mix}}} \rfloor} + (2\delta + \frac{\psi}{S+1} + D_\Omega \mathbb{P}[\|\mathbf{z}\| > \varphi_0])(C + \frac{D_\Omega}{\eta_0})^{S+1} + D_\Omega \mathbb{P}[T < \tau_\epsilon].
\end{aligned}$$

Letting ψ go to 0,

$$\begin{aligned}
\text{(B.16)} \qquad W_2(X_{T+S}, \pi) &\leq D_\Omega 2^{-\lfloor \frac{S}{\tau_{\text{mix}}} \rfloor} + (2\delta + D_\Omega \mathbb{P}[\|\mathbf{z}\| > \varphi_0])(C + \frac{D_\Omega}{\eta_0})^{S+1} \\
&+ D_\Omega \mathbb{P}[T < \tau_\epsilon].
\end{aligned}$$

For $\alpha \in \mathbb{N}$, define $\delta(\alpha) = \frac{1}{\alpha^2}$, $\varphi_0(\alpha) = \inf\{\varphi : \mathbb{P}[\|\mathbf{z}\| > \varphi] \leq \alpha^{-2}\}$, $S(\alpha) = \lfloor \frac{-\log(\alpha)}{\log(C + \frac{D_\Omega}{\eta_0})} \rfloor - 1$, and $T(\alpha)' = \inf\{t : \mathbb{P}[t < \tau_{\epsilon(\delta(\alpha))}] \leq \frac{1}{\alpha}\}$. It is easy to check that $\lim_{\alpha \to \infty} S(\alpha) = \lim_{\alpha \to \infty} T(\alpha)' = \infty$, and so for any sequence $T(\alpha) > T(\alpha)'$ inequality (B.16) implies

$$\lim_{\alpha \to \infty} W_2(X_{T(\alpha)+S(\alpha)}, \pi) \leq \lim_{\alpha \to \infty} (D_\Omega 2^{-\lfloor \frac{S(\alpha)}{\tau_{\text{mix}}} \rfloor} + \frac{4D_\Omega}{\alpha}) = 0.$$

Since this holds for *any* sequence $T(\alpha) > T(\alpha)'$, inequality (4.5) follows.[3] ■

[3]Since the convergence to stationarity under the Wasserstein distance may not be monotone, this flexibility in the choice of $T(\alpha)$ is necessary to obtain the desired convergence result.

Proof of Theorem 4.8. It is enough to check that the conditions of Theorem 4.6 hold. Going through the elements of Definition 4.5 in order:

1. To check that inequality (4.2) holds, fix $\delta > 0$. By results in [9],[4] there exists a constant $\epsilon_1 = \epsilon_1(\delta, \lambda) > 0$ so that for all $\epsilon < \epsilon_1$

$$\sup_{\theta \in \Theta} |p_{\mathcal{S}}(\theta) - p(\theta|\mathbf{d})| < \frac{\delta}{2D_\Omega} \tag{B.17}$$

if $\mathcal{S}$ is an ϵ-cover and the points $\mathcal{B}(\theta, R)$ chosen in Step 2 of Algorithm A.4 are λ-poised. The same discussion in [9] implies that there exists a constant $\epsilon_2 = \epsilon_2(\delta, \lambda) > 0$ so that for all $\epsilon < \epsilon_2$,

$$\sup_{\theta \in \Theta} |M_{\mathcal{S}}(\theta) - M_\infty(\theta)|,\ |\nabla_\theta(\pi_{\mathcal{S}}) - \nabla_\theta(\pi_\infty)| < \delta \tag{B.18}$$

if $\mathcal{S}$ is an ϵ-cover and the points $\mathcal{B}(\theta, R)$ chosen in Step 2 of Algorithm A.4 are λ-poised. Since the smallest singular value of $M(\theta)$ is bounded below uniformly in θ, this implies that there exists a constant $\epsilon_3 = \epsilon_3(\delta, \lambda) > 0$ so that for all $\epsilon < \epsilon_3$ (see [21, Prop. 7]),

$$\sup_{\theta \in \Theta} W_2(q_{\mathcal{S}}(\theta, \cdot), q_\infty(\theta, \cdot)) < \frac{\delta}{2} \tag{B.19}$$

as long as $\mathcal{S}$ is an ϵ-cover and the points $\mathcal{B}(\theta, R)$ chosen in Step 2 of Algorithm A.4 are λ-poised.
Combining inequalities (B.17) and (B.19), we have for all $0 < \epsilon < \min(\epsilon_1, \epsilon_3)$ that

$$\begin{aligned}\sup_{\theta \in \Theta} W_2(K_{\mathcal{S}}(\theta, \cdot), K_\infty(\theta, \cdot)) &\leq \sup_{\theta \in \Theta} W_2(q_{\mathcal{S}}(\theta, \cdot), q_\infty(\theta, \cdot)) + D_\Omega \sup_{\theta \in \Theta} |p_{\mathcal{S}}(\theta) - p(\theta|\mathbf{d})| \\ &\leq \frac{\delta}{2} + \frac{\delta}{2} = \delta.\end{aligned}$$

This completes the proof of inequality (4.2).

2. By the assumption that the mass matrix $M(\theta)$ and likelihood $\ell(\theta|\mathbf{d}, \mathbf{f})$ are both C^∞ functions on Ω, and that the smallest singular value of M and the likelihood ℓ are both uniformly bounded away from zero, we have

$$\begin{aligned}\|q_\infty(\theta, \cdot) - q_\infty(\theta', \cdot)\|_{\mathrm{TV}} &= \left\| \mathcal{N}\left(\theta + \frac{\epsilon}{2} M(\theta) \nabla_\theta \log\left(\ell(\theta|\mathbf{d}, \mathbf{f}) p(\theta)\right), \epsilon M(\theta)\right)\right. \\ &\qquad \left. - \mathcal{N}\left(\theta' + \frac{\epsilon}{2} M(\theta') \nabla_\theta \log\left(\ell(\theta'|\mathbf{d}, \mathbf{f}) p(\theta')\right), \epsilon M(\theta')\right) \right\|_{\mathrm{TV}} \\ &\leq \left\| \mathcal{N}\left(\theta + \frac{\epsilon}{2} M(\theta) \nabla_\theta \log\left(\ell(\theta|\mathbf{d}, \mathbf{f}) p(\theta)\right), \epsilon M(\theta)\right)\right. \\ &\qquad \left. - \mathcal{N}\left(\theta' + \frac{\epsilon}{2} M(\theta') \nabla_\theta \log\left(\ell(\theta'|\mathbf{d}, \mathbf{f}) p(\theta')\right), \epsilon M(\theta)\right) \right\|_{\mathrm{TV}} \\ &\quad + \left\| \mathcal{N}\left(\theta' + \frac{\epsilon}{2} M(\theta') \nabla_\theta \log\left(\ell(\theta'|\mathbf{d}, \mathbf{f}) p(\theta')\right), \epsilon M(\theta)\right)\right.\end{aligned} \tag{B.20}$$

[4] The required result is a combination of Theorems 3.14 and 3.16, as discussed in the text after the proof of Theorem 3.16 of [9].

$$- \mathcal{N}\left(\theta' + \frac{\epsilon}{2} M(\theta') \nabla_\theta \log\left(\ell(\theta'|\mathbf{d},\mathbf{f}) p(\theta')\right), \epsilon M(\theta')\right)\Big\|_{\mathrm{TV}}$$
$$= O_c(\|\theta - \theta'\|),$$

where the bound on the first term in the last line is standard, and the second term in the last line is bounded by an application of [26, Lem. 4.8]. By a similar calculation,

$$|\alpha_\infty(\theta, z) - \alpha_\infty(\theta', z)| = O_c(\|\theta - \theta'\|). \tag{B.21}$$

Inequalities (B.20) and (B.21) imply that

$$\begin{aligned}\sup_{\theta,\theta'\in\Theta,\, \|\theta-\theta'\|<\eta} W_2(K_\infty(\theta,\cdot), K_\infty(\theta',\cdot)) &\le D_\Omega \sup_{\theta,\theta'\in\Theta,\, \|\theta-\theta'\|<\eta} \|K_\infty(\theta,\cdot) - K_\infty(\theta',\cdot)\|_{\mathrm{TV}} \\ &\le D_\Omega\Big(\sup_{\theta,\theta'\in\Theta,\, \|\theta-\theta'\|<\eta} \|q_\infty(\theta,\cdot) - q_\infty(\theta',\cdot)\|_{\mathrm{TV}} + \sup_{\theta,\theta',z\in\Theta,\, \|\theta-\theta'\|<\eta} |\alpha_\infty(\theta,z) - \alpha_\infty(\theta',z)|\Big) \\ &= O(\|\theta - \theta'\|).\end{aligned}$$

This completes the proof of inequality (4.3).

3. Inequality (4.4) follows immediately from (B.17) and (B.18).
4. The first item in Assumption 3.1 holds by our assumption that Θ is the d-dimensional torus.
5. The second item in Assumption 3.1 has two parts. The first part, that $p(\cdot|\mathbf{d})$ has a C^∞ density that is bounded away from zero uniformly in θ, is an assumption of our theorem. The second part, that $q(\theta,\cdot|\mathbf{f})$ has C^∞ density that is bounded away from zero uniformly in $\theta, \mathbf{f}$, follows from the form of the mMALA proposal and the fact that the state space is compact.
6. Items 3 through 6 in Assumption 3.1 are assumed in the statement of the theorem.

This completes the proof of the theorem. ■

REFERENCES

[1] R. J. Adler, *The geometry of random fields*, SIAM, 1981.

[2] Myles R Allen, Vicente R Barros, John Broome, Wolfgang Cramer, Renate Christ, John A Church, Leon Clarke, Qin Dahe, Purnamita Dasgupta, Navroz K Dubash, et al., *IPCC fifth assessment synthesis report-climate change 2014 synthesis report*, (2014).

[3] Nikolay Bliznyuk, David Ruppert, and Christine A. Shoemaker, *Local Derivative-Free Approximation of Computationally Expensive Posterior Densities*, Journal of Computational and Graphical Statistics, 21 (2012), pp. 476–495.

[4] Stephen P Brooks and Gareth O Roberts, *Assessing Convergence of Markov Chain Monte Carlo Algorithms*, Statistics and Computing, 8 (1998), pp. 319–335.

[5] B. Calderhead, *A general construction for parallelizing Metropolis-Hastings algorithms*, Proceedings of the National Academy of Sciences, 111 (2014), pp. 17408–17413.

[6] Olivier Cappe, Arnaud Guillin, Jean-Michel Marin, and Christian P. Robert, *Population Monte Carlo*, Journal of Computational and Graphical Statistics, 13 (2004), pp. 907–929.

[7] P. Chen and Ch. Schwab, *Sparse-grid, reduced-basis Bayesian inversion*, Computer Methods in Applied Mechanics and Engineering, 297 (2015), pp. 84–115.

[8] J. Andrés Christen and Colin Fox, *Markov chain Monte Carlo Using an Approximation*, Journal of Computational and Graphical Statistics, 14 (2005), pp. 795–810.

[9] Andrew R. Conn, Katya Scheinberg, and Luís N. Vicente, *Introduction to Derivative-Free Optimization*, SIAM, 2009.

[10] Patrick R Conrad, Youssef M Marzouk, Natesh S Pillai, and Aaron Smith, *Asymptotically exact MCMC algorithms via local approximations of computationally intensive models*, Journal of the American Statistical Association, in press (2015). arXiv:1402.1694.

[11] S. L. Cotter, M. Dashti, and A. M. Stuart, *Approximation of Bayesian Inverse Problems*, SIAM Journal of Numerical Analysis, 48 (2010), pp. 322–345.

[12] Mary Kathryn Cowles and Bradley P Carlin, *Markov Chain Monte Carlo Convergence Diagnostics : A Comparative Review*, Journal of the American Statistical Association, 91 (1996), pp. 883–904.

[13] Radu V. Craiu, Jeffrey Rosenthal, and Chao Yang, *Learn From Thy Neighbor : Parallel-Chain and Regional Adaptive MCMC*, Journal of the American Statistical Association, 104 (2009), pp. 1454–1466.

[14] T. Cui, C. Fox, and M. J. O'Sullivan, *Bayesian calibration of a large-scale geothermal reservoir model by a new adaptive delayed acceptance Metropolis Hastings algorithm*, Water Resources Research, 47 (2011), p. W10521.

[15] T. Cui, Y. M. Marzouk, and K. Willcox, *Scalable posterior approximations for large-scale Bayesian inverse problems via likelihood-informed parameter and state reduction*, Journal of Computational Physics, 315 (2016), pp. 363–387.

[16] M Dashti and AM Stuart, *Uncertainty Quantification and Weak Approximation of an Elliptic Inverse Problem*, SIAM Journal of Numerical Analysis, 49 (2011), pp. 2524–2542.

[17] Jules Dupuit, *Etudes theoriques et pratiques sur le mouvement des eaux dans les canaux decouverts et a travers les terrains permeables*, Dunod, 1863.

[18] James Allen Fill and Mark Huber, *The randomness recycler: a new technique for perfect sampling*, in Foundations of Computer Science, 2000. Proceedings. 41st Annual Symposium on, IEEE, 2000, pp. 503–511.

[19] P Fretwell, Hamish D Pritchard, David G Vaughan, JL Bamber, NE Barrand, R Bell, C Bianchi, RG Bingham, DD Blankenship, G Casassa, et al., *Bedmap2: improved ice bed, surface and thickness datasets for Antarctica*, The Cryosphere, 7 (2013), pp. 375–393.

[20] Mark Girolami and Ben Calderhead, *Riemann manifold langevin and hamiltonian monte carlo methods*, Journal of the Royal Statistical Society: Series B (Statistical Methodology), 73 (2011), pp. 123–214.

[21] C. R. Givens and R. M. Shortt, *A class of Wasserstein metrics for probability distributions*, Michigan Mathematical Journal, 31 (1984), pp. 231–240.

[22] Heikki Haario, Eero Saksman, and Johanna Tamminen, *An adaptive Metropolis algorithm*, Bernoulli, 7 (2001), pp. 223–242.

[23] Intergovernmental Panel on Climate Change, *Climate Change 2013: The Physical Science Basis: Working Group I Contribution to the Fifth Assessment Report of the Intergovernmental Panel on Climate Change*, Cambridge University Press, 2014.

[24] V. Roshan Joseph, *Bayesian Computation Using Design of Experiments-Based Interpolation Technique*, Technometrics, 54 (2012), pp. 209–225.

[25] M.C. Kennedy and A. O'Hagan, *Bayesian calibration of computer models*, Journal of the Royal Statistical Society: Series B (Statistical Methodology), 63 (2001), pp. 425–464.

[26] B. Klartag, *A central limit theorem for convex sets*, Inventiones Mathematicae, 168 (2007), pp. 91–131.

[27] Jinglai Li and Youssef M. Marzouk, *Adaptive construction of surrogates for the Bayesian solution of inverse problems*, SIAM Journal on Scientific Computing, 36 (2014), pp. A1163–A1186.

[28] Jilu Li, John Paden, Carl Leuschen, Fernando Rodriguez-Morales, Richard D Hale, Emily J Arnold, Reid Crowe, Daniel Gomez-Garcia, and Prasad Gogineni, *High-altitude radar measurements of ice thickness over the Antarctic and Greenland ice sheets as a part of Operation IceBridge*, IEEE Transactions on Geoscience and Remote Sensing, 51 (2013), pp. 742–754.

[29] Douglas R MacAyeal, *Large-scale ice flow over a viscous basal sediment: Theory and application to ice stream B, Antarctica*, Journal of Geophysical Research: Solid Earth (1978–2012), 94 (1989), pp. 4071–4087.

[30] ———, *A tutorial on the use of control methods in ice-sheet modeling*, J. Glaciol, 39 (1993), pp. 91–98.

[31] ———, *EISMINT: Lessons in ice-sheet modeling*, Department of Geophysical Sciences, University of Chicago, Chicago, IL, 1832 (1997), p. 1839.

[32] James Martin, Lucas C Wilcox, Carsten Burstedde, and Omar Ghattas, *A stochastic Newton MCMC method for large-scale statistical inverse problems with application to seismic inversion*, SIAM Journal on Scientific Computing, 34 (2012), pp. 1460–1487.

[33] Youssef Marzouk and Dongbin Xiu, *A stochastic collocation approach to Bayesian inference in inverse problems*, Communications in Computational Physics, 6 (2009), pp. 826–847.

[34] Youssef M. Marzouk, Habib N. Najm, and Larry A. Rahn, *Stochastic spectral methods for efficient Bayesian solution of inverse problems*, Journal of Computational Physics, 224 (2007), pp. 560–586.

[35] L Shawn Matott, *Screening-Level Sensitivity Analysis for the Design of Pump-and-Treat Systems*, Ground Water Monitoring and Remediation, 32 (2012), pp. 66–80.

[36] Noemi Petra, James Martin, Georg Stadler, and Omar Ghattas, *A computational framework for infinite-dimensional Bayesian inverse problems, part II: stochastic Newton MCMC with application to ice sheet flow inverse problems*, SIAM Journal on Scientific Computing, 36 (2014), pp. A1525–A1555.

[37] Noemi Petra, Hongyu Zhu, Georg Stadler, Thomas JR Hughes, and Omar Ghattas, *An inexact Gauss–Newton method for inversion of basal sliding and rheology parameters in a nonlinear Stokes ice sheet model*, Journal of Glaciology, 58 (2012), pp. 889–903.

[38] James Gary Propp and David Bruce Wilson, *Exact sampling with coupled Markov chains and applications to statistical mechanics*, Random Structures and Algorithms, 9 (1996), pp. 223–252.

[39] Carl Edward Rasmussen, *Gaussian Processes to Speed up Hybrid Monte Carlo for Expensive Bayesian Integrals*, in Bayesian Statistics 7, Oxford University Press, 2003, pp. 651–659.

[40] Gareth O Roberts and Jeffrey S Rosenthal, *One-shot coupling for certain stochastic recursive sequences*, Stochastic processes and their applications, 99 (2002), pp. 195–208.

[41] Jeffrey S Rosenthal, *Parallel computing and Monte Carlo algorithms*, Far east journal of theoretical statistics, 4 (2000), pp. 207–236.

[42] Jerome Sacks, William J. Welch, Toby J. Mitchell, and Henry P. Wynn, *Design and analysis of computer experiments*, Statistical Science, 4 (1989), pp. 409–423.

[43] Thomas J. Santner, Brian J. Williams, and William I. Notz, *The Design and Analysis of Computer Experiments*, Springer, New York, 2003.

[44] B.E. Schutz, H.J. Zwally, C.A. Shuman, D. Hancock, and J.P. DiMarzio, *Overview of the ICESat mission*, Geophysical Research Letters, 32 (2005).

[45] David Steinsaltz, *Locally contractive iterated function systems*, Annals of Probability, (1999), pp. 1952–1979.

[46] Cédric Villani, *Optimal transport: old and new*, vol. 338, Springer Science & Business Media, 2008.